

SCHOOL OF
CIVIL ENGINEERING

INDIANA

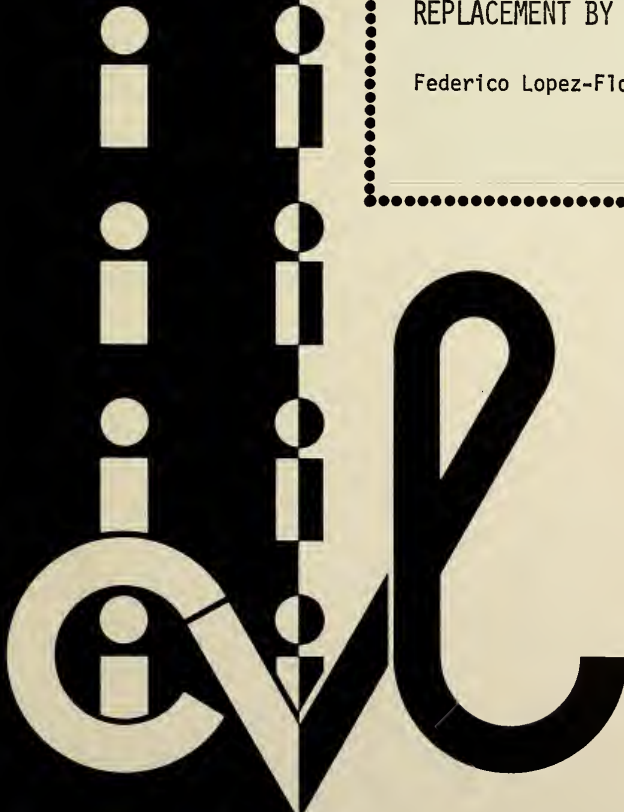
DEPARTMENT OF HIGHWAYS

JOINT HIGHWAY RESEARCH PROJECT

JHRP-82-11

FLYASH AND EFFECTS OF PARTIAL CEMENT
REPLACEMENT BY FLYASH

Federico Lopez-Flores



PURDUE UNIVERSITY



JOINT HIGHWAY RESEARCH PROJECT

JHRP-82-11

FLYASH AND EFFECTS OF PARTIAL CEMENT
REPLACEMENT BY FLYASH

Federico Lopez-Flores



Informational Report

TO: Mr. Robert L. Eskew, Chairman
Joint Highway Research Project

July 13, 1982

FROM: Harold L. Michael, Director
Joint Highway Research Project

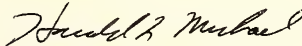
File: 5-12

The attached research report has been duplicated by JHRP for the information of the Indiana Department of Highways. The research was primarily supported by the U.S. Department of Energy. The Report is titled "Flyash and Effects of Partial Cement Replacement by Flyash". It has been authored by Mr. Federico Lopez-Flores under the direction of Professor Sidney Diamond of our faculty.

As flyash use in concrete is now becoming common because of current and projected economic factors and possible technical benefits to concrete performance its increased use in Indiana may be anticipated. The findings of this research should be of value to Department of Highways personnel in implementing this use in Indiana.

The report is presented as information for use where applicable.

Sincerely,



Harold L. Michael
Director

HLM:ms

cc: A. G. Altschaeffl
J. M. Bell
W. L. Dolch
R. L. Eskew
J. D. Fricker
G. D. Gibson
W. H. Goetz

G. K. Hallock
J. F. McLaughlin
R. D. Miles
P. L. Owens
B. K. Partridge
G. T. Satterly

C. F. Scholer
R. M. Shanteau
K. C. Sinha
C. A. Venable
L. E. Wood
E. J. Yoder
S. R. Yoder

Informational Report
FLYASH AND EFFECTS OF PARTIAL CEMENT
REPLACEMENT BY FLYASH

by

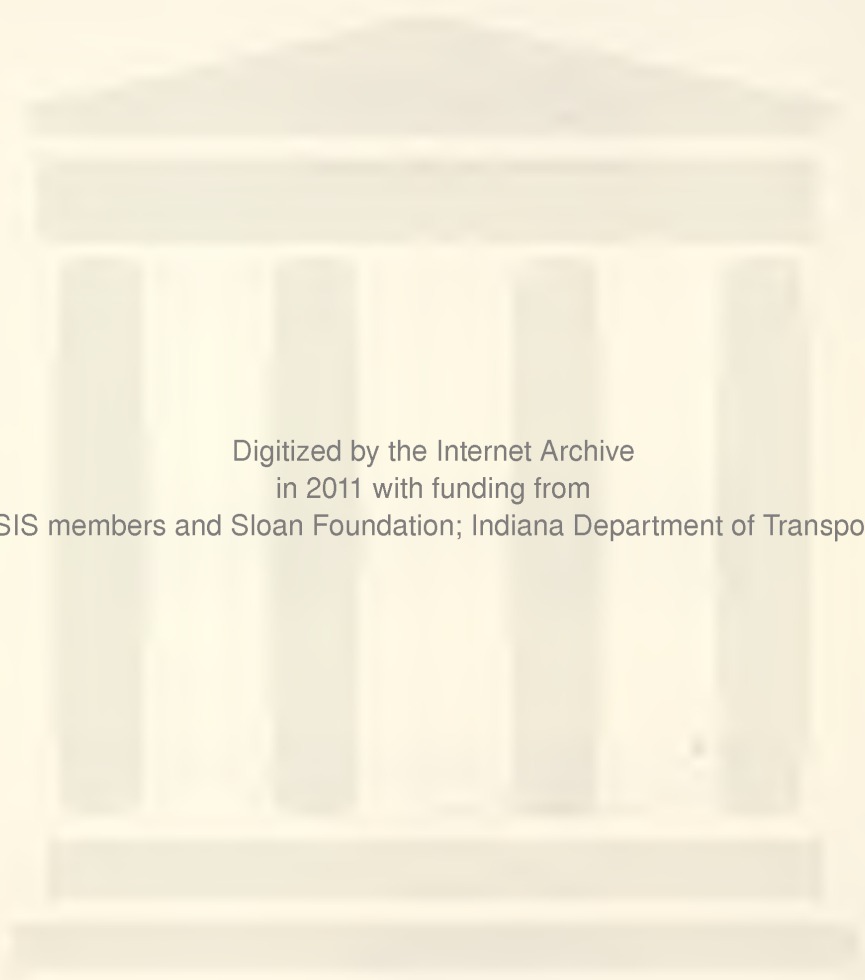
Federico Lopez-Flores
Graduate Instructor in Research
School of Civil Engineering

File: 5-12

This research was performed by the author in partial fulfillment of the requirements for the Degree of Master of Science. Much of the research was supported by the U.S. Department of Energy, through its Project DE-AC02-78cs 40222.

Copies of the Report have been prepared by the Joint Highway Research Project for the information of the Indiana Department of Highways.

Purdue University
West Lafayette, Indiana
July 13, 1982



Digitized by the Internet Archive
in 2011 with funding from
LYRASIS members and Sloan Foundation; Indiana Department of Transportation

ACKNOWLEDGMENTS

The author wishes to express his appreciation to Professor S. Diamond for his guidance and patience throughout this study. He would also like to thank the other members of his advisory committee, Professor C. F. Scholer and Professor D. N. Winslow.

The assistance of Mrs. Janet Lovell is gratefully acknowledged.

Much of this work was supported by the U.S. Department of Energy Project DE-ACO2-78cs 40222. Gratitude is also due to the Consejo Nacional de Ciencia y Tecnologia, Mexico.

TABLE OF CONTENTS

	Page
LIST OF TABLES	vi
LIST OF FIGURES	ix
ABSTRACT	xii
CHAPTER 1 - INTRODUCTION	1
General Aspects	1
Characterization of Coal	3
Flyash Production	4
Morphology of Flyash	6
Physical Characteristics	7
Pozzolanic Reaction	8
Effects of Flyash on Concrete	10
Heat Evolution	13
Flyash and Alkali-Aggregate Reaction	14
CHAPTER 2 - MATERIALS USED IN THIS STUDY	16
Reference Cement	16
Flyashes	17
CHAPTER 3 - EXPERIMENTAL METHODS AND TECHNIQUES	19
Loss on Ignition	19
Specific Gravity	19
Particle Size Distribution	20
X-Ray Diffraction	20
Semiquantitative Analysis by Energy Dispersive X-Ray Analysis	21
Mixing Procedure for Pastes	24
Setting Time	24
Temperature Evolution	24
Expression of Pore Solution from Pastes	25
Non-Evaporable Water Determinations	29
Chemical Analyses of Pore Solutions	29
Mixing Procedure for Mortar and Preparation of Mortar Cubes	31
Compressive Strength Tests of Mortar Cubes	31

	Page
Mixing Procedure for Mortar and Preparation of Mortar Bars	31
Storage and Observation of Length Changes in Mortar Bars	32
Mix Design for Concrete and Casting of 3 X 6 in Cylinders	32
Compressive Strength Tests of Concrete Cylinders	33
 CHAPTER 4 - RESULTS AND DISCUSSION	
Loss on Ignition	34
Specific Gravity	34
Particle Size Distributions	36
X-Ray Diffraction	39
Semiquantitative Analysis by Energy Dispersive X-Ray Analysis	46
Setting Time	62
Temperature Evolution	63
Non-Evaporable Water Determinations	66
Chemical Analyses of Pore Solutions	69
Compressive Strength of Mortar Cubes	82
Length Changes in Mortar Bars	82
Compressive Strength of Concrete Cylinders	93
 CHAPTER 5 - CONCLUSIONS	98
 BIBLIOGRAPHY	100
 APPENDICES	
Appendix A. Chemical Composition of Flyash C ..	105
Appendix B. X-Ray Diffraction Patterns of the Flyashes Used	106
Appendix C. Chemical Analyses of Paste Pore Solutions	111
Appendix D. Length Change Results for Mortar Bars	117

LIST OF TABLES

Table	Page
2- 1. Chemical composition of reference cement	16
2- 2. Source and classification of flyashes	17
2- 3. Chemical composition of flyashes, percentage .	18
3- 1. Mix designs for cement-flyash concrete systems and reference concrete	33
4- 1. Ignition loss determinations of flyashes	35
4- 2. Measured values of specific gravity of flyashes	35
4- 3. Stated percentile diameters representing the size distributions on the flyashes, m.	36
4- 4. Crystalline components identified in the flyashes	41
4- 5. Weighted mean peak intensity ratio of each element to silicon in flyash A as compared to the corresponding overall ratio	52
4- 6. Weighted mean peak intensity ratio of each element to silicon in flyash B as compared to the corresponding overall ratio	53
4- 7. Weighted mean peak intensity ratio of each element to silicon in flyash D as compared to the corresponding overall ratio	54
4- 8. Setting times for cement-flyash pastes	62
4- 9. Temperature evolution maxima compared to time of set in cement-flyash pastes	67
4-10. Non-evaporable water content in cement-flyash pastes at different ages, percent	68

Table	Page
4-11. Measured normality of ionic species in paste pore solutions as a function of time (adjusted for change in water content)	70
4-12. Compressive strength of mortar cubes prepared with different flyashes, Psi, and corresponding standard deviations shown in parentheses.	83
4-13. Water-soluble alkalies in cement and flyashes used	93
4-14. Compressive strength of 3X6 in concrete cylinders prepared with different flyashes, Psi, and corresponding standard deviations shown in parentheses	94
 Appendix	
Table	
A- 1. Wet chemical analysis of flyash C	105
C- 1. Measured normality of ionic species in paste pore solutions as a function of time (not adjusted for change in water content). Reference Portland Cement Paste	111
C- 2. Measured normality of ionic species in paste pore solutions as a function of time (not adjusted for change in water content). Paste with Flyash A	112
C- 3. Measured normality of ionic species in paste pore solutions as a function of time (not adjusted for change in water content). Paste with Flyash B	113
C- 4. Measured normality of ionic species in paste pore solutions as a function of time (not adjusted for change in water content). Paste with Flyash C	114
C- 5. Measured normality of ionic species in paste pore solutions as a function of time (not adjusted for change in water content). Paste with Flyash D	115

Table	Page
C- 6. Measured normality of ionic species in paste pore solutions as a function of time (not adjusted for change in water content). Paste with Flyash E	116
D- 1. Length changes in reference portland cement mortar bars, percent strain	117
D- 2. Length changes in system A cement-flyash mortar bars, percent strain	118
D- 3. Length changes in system B cement-flyash mortar bars, percent strain	119
D- 4. Length changes in system C cement-flyash mortar bars, percent strain	120
D- 5. Length changes in system D cement-flyash mortar bars, percent strain	121
D- 6. Length changes in system E cement-flyash mortar bars, percent strain	122

LIST OF FIGURES

Figure	Page
3- 1. Scheme for selecting spots for analysis on flyash spheres	22
3- 2. Millipore pressure filtering system used to obtain pore solution from cement pastes	27
3- 3. Isometric half-section of the pore solution expression apparatus	28
4- 1. Particle size distribution of flyashes A, B, and C	37
4- 2. Particle size distribution of flyashes D and E	38
4- 3. Effect of glass content on the x-ray pattern of each flyash studied	45
4- 4. Semiquantitative peak intensity ratio of elements to silicon in flyash A	47
4- 5. Semiquantitative peak intensity ratio of elements to silicon in flyash B	48
4- 6. Semiquantitative peak intensity ratio of elements to silicon in flyash D	49
4- 7. Micrograph of flyash A particle at 1000X magnification	56
4- 8. Micrograph of flyash A particle at 3000X magnification	57
4- 9. Micrograph of flyash B particle at 1000X magnification	58
4-10. Micrograph of a flyash D plerosphere at 1000X magnification	59

Figure	Page
4-11. Micrograph of flyash D particle at 7000X magnification	60
4-12. Micrograph of "fused" flyash D particles at 1500X magnification	61
4-13. Temperature increase in cement-flyash pastes and reference cement paste	64
4-14. Temperature increase in cement-flyash pastes and reference cement paste during the first four hours of hydration	65
4-15. Concentration of ions in reference cement paste pore solution as a function of time	73
4-16. Concentration of ions in system A paste pore solution as a function of time	75
4-17. Concentration of ions in system B paste pore solution as a function of time	77
4-18. Concentration of ions in system C paste pore solution as a function of time	78
4-19. Concentration of ions in system D paste pore solution as a function of time	80
4-20. Concentration of ions in system E paste pore solution as a function of time	81
4-21. Compressive strengths of mortar cubes bearing flyashes A, B, and C	84
4-22. Compressive strengths of mortar cubes bearing flyashes D and E	85
4-23. Length change of reference cement mortar bars	87
4-24. Length change of system A mortar bars	88
4-25. Length change of system B mortar bars	89
4-26. Length change of system C mortar bars	90
4-27. Length change of system D mortar bars	91
4-28. Length change of system E mortar bars	92

Figure	Page
4-29. Compressive strengths of concrete cylinders bearing flyashes A, B, and C	96
4-30. Compressive strengths of concrete cylinders bearing flyashes D and E	97
Appendix	
Figure	
B- 1. X-ray diffraction pattern for flyash A	106
B- 2. X-ray diffraction pattern for flyash B	107
B- 3. X-ray diffraction pattern for flyash C	108
B- 4. X-ray diffraction pattern for flyash D	109
B- 5. X-ray diffraction pattern for flyash E	110

ABSTRACT

Lopez-Flores, Federico. M.S., Purdue University, May 1982.
Flyash and Effects of Partial Cement Replacement by Flyash.
Major Professor: Sidney Diamond.

The main objective of this work was to study the effects of partial cement replacement by flyash. Through these studies, done on paste, mortar, and concrete, it is hoped to gain a better understanding of the behavior of flyash in a concrete mix.

An important part of this work was an extensive and detailed characterization of five flyashes (3 ASTM class C and 2 class F materials). This included chemical determinations, particle size distribution measurements, specific gravity determinations, detailed x-ray diffraction studies, study of particle morphology by scanning electron microscopy, and chemical analyses of individual flyash particles of various sizes by energy dispersive x-ray analysis methods. It was found from x-ray diffraction that the high-lime (class C) flyashes studied have a more complex crystalline composition and different glass characteristics than the low-lime (class F) flyashes studied.

A number of studies of the effects of these flyashes on the behavior of cement pastes, mortars, and concretes were also carried out. In these studies a standard 30 percent weight-for-weight replacement of cement by flyash, and a standard water to cementitious solids (cement plus flyash) ratio of 0.50 were used.

The setting times, temperature increases during hydration, and the ionic compositions of pore solutions were studied for flyash-cement pastes. Some correlations were made between the results obtained in these experiments and the observed results of compressive strength determinations of mortar cubes and concrete cylinders prepared with the corresponding flyashes.

Mortar bars were prepared to observe the effects of flyash on a potential alkali-aggregate reaction, using Beltane opal as the reactive aggregate. Expansion was observed in mortar bars made using flyash in which the sum of the water-soluble alkalis in the flyash plus those in the cement exceeded about 0.7 percent equivalent Na_2O .

CHAPTER 1

INTRODUCTION

General Aspects

Flyash is currently being used in many places as a constituent of portland cement concrete, replacing part of the portland cement that would otherwise be used.

There is a distinct need for understanding the effects produced by various flyashes in such use. Present knowledge of the chemical and physical effects produced by flyashes is relatively superficial, in part due to a failure to appreciate the detailed characteristics of individual flyashes and the difference between different flyashes.

The main objective of this work was to characterize a suite of 5 different flyashes (3 ASTM class C and 2 ASTM class F materials) and to study and compare their effects in standard paste, mortar, and concrete formulations.

Flyash is a byproduct of the combustion of pulverized coal in thermoelectric power plants. The particles are typically spherical, with diameters falling between <1 and $150 \mu\text{m}$, allowing them to be carried by flue gases. The flyash particles are collected with mechanical or electrostatic precipitators before the gases are discharged into the atmosphere.

The earliest use of flyash in concrete construction was in massive structures like dams. In the beginning the advantages derived from this use were both of economic and technical importance. With a weight-for-weight replacement of cement by flyash of between 20 and 40 percent, the cost per cubic yard of concrete

was substantially lowered. On the technical side a much-desired reduction in the early heat evolution during hydration was achieved. These advantages were supplemented by the fact that strength development was similar or better at 28 days to that of conventional concrete, despite the slightly lower strengths at earlier ages.

In 1934 McMillan and Powers (1) reported results of a study on admixtures where two precipitator flyashes were included. A more extensive investigation and one solely dedicated to flyash was published in 1937 by Davis et al. (2) in an attempt to rationalize the use of flyash in concrete. In the accompanying discussion of the cited paper C. P. Derleth pointed out that "...many thousands of tons of flyash have actually been used in a wide variety of concrete structures". It appears that flyash was used totally on an empirical basis before any research was done on this subject.

In spite of substantial research since that time, even today the use of flyash in concrete is less than it might be, due to the general observations that flyash reduces initial strength and that it delays the time at which the forms may be stripped. Nevertheless, many workers have found beneficial effects of flyash in concrete. Lovewell and Washa (3) concluded that concrete of a given ultimate strength and durability could be produced by replacing as much as 30 to 50 percent of the cement originally required by flyash of suitable fineness and composition.

Mielenz (4) pointed out certain beneficial and detrimental aspects of flyash in concrete. Some positive aspects include increased strength for a given cement content, a more uniform development of strength, lower heat evolution, reduced alkali-aggregate reaction, resistance to chemical attack in consequence of reduced permeability and absorption, and lower costs per unit volume for a given quality. On the other hand, concretes made with flyash show slow early strength gain, especially if curing conditions are not adequate. The control of air content is sometimes more difficult when flyash is included in concrete. Another drawback is a possibly reduced resistance to freezing and thawing.

The future may see increasing amounts of flyash being used in concrete to the extent that flyash might come to be considered a normal ingredient of concrete. The economic advantages of using flyash as well as the growing knowledge of the behavior of flyash in concrete make this a reasonable assumption.

Characterization of Coal

Coal, as it is used in power plants, contains various inorganic impurities. Some are intrinsic to the material either because of coincidental sedimentation, or because they formed part of the composition of the coal-forming material itself. Other impurities have been deposited subsequently to the formation of coal through geologic activity. Finally there are impurities that are related to the mining activity proper.

The American Society for Testing and Materials (ASTM) (5) has classified coal based on fixed carbon and caloric value into four classes, viz., anthracite, bituminous, subbituminous, and lignite. Each class is further divided into groups.

Mazza and Wilson (6) studied coal used in power plants and classified coal minerals into five groups:

Aluminosilicates	Kaolinite	$\text{Al}_2\text{Si}_2\text{O}_5(\text{OH})_4$
	Illite	$\text{K}(\text{Si}_3 \cdot \text{Al})\text{Al}_{10}\text{O}_{10}(\text{OH})_4$
Carbonates	Siderite	FeCO_3
	Calcite	CaCO_3
	Dolomite	$\text{CaMg}(\text{CO}_3)_2$
Sulfides	Pyrite and Marcasite	FeS_2
Silica	Quartz	SiO_2
Accessory minerals	Feldspars	$(\text{K}, \text{Na})\text{AlSi}_3\text{O}_8$
		$\text{CaAl}_2\text{Si}_2\text{O}_8$
	Gypsum	$\text{CaSO}_4 \cdot 2\text{H}_2\text{O}$

These minerals contain the major elements found in flyash (Si, Al, Ca, Fe, S, K, Na, Ti, and Mg) (7, 8). The mineral matter usually represents from 5 to 25 percent of the weight of the coal. The occurrence of these minerals in coal is as discrete grains, with a mass median diameter of around 2 μm ; however some are as big as 15 μm (7).

The flyashes produced by the combustion of coals have been classified by ASTM (9) into two classes which depend directly on which coal is used. Flyash class F is normally produced when anthracite or bituminous coal is burned. Flyash class C is normally produced if subbituminous or lignitic coal is burned. ASTM has set the following requirements for each of these flyashes:

	Percent	
	F	C
($\text{SiO}_2 + \text{Al}_2\text{O}_3 + \text{Fe}_2\text{O}_3$), min.	70	50
SO_3 , max.	5	5
Moisture content, max.	3	3
Loss on ignition, max.	12	6

Flyash Production

The coal burning process involves extremely rapid heating to favor complete combustion of most of the carbonaceous material. The mineral matter undergoes complex reactions in what Gibbon (7) has called "flash melting" accompanied by some vaporization. He pointed out that the fact that pulverized coal is generally very fine and that the heating period is brief provoke rapid cooling involving

quenching and crystallization with surface condensation of some of the vaporized phases. Gibbon considered that this vapor deposition could have leaching effects on the newly formed flyash particles, and that the balance between crystal and glass phases largely controls solubility of flyash. The results of Watt and Thorne (10) on British flyashes can be generalized to at least some other flyashes. They found the crystalline phases to account for 11 to 17 percent of the flyash with 71 to 88 percent corresponding to the glassy phases.

Several workers (6, 7, 10, 11, 12) have reported the presence of quartz, hematite, magnetite, mullite, lime, and anhydrite in the crystalline phases of flyash. Gibbon (7) described a large glass "hump" over which the patterns of these components appear in x-ray diffraction analysis. Mitchell and Gluskoter (13) suggested that the mineralogy of flyash depends on the burning conditions of the power plant. They studied equilibrium phases at different temperatures up to almost complete melting of the flyash. From this work they concluded that for their flyashes mullite ($3\text{Al}_2\text{O}_3 \cdot 2\text{SiO}_2$) was the final equilibrium crystalline phase coexisting with the liquid phase.

The sulfur content of a coal is a serious problem for power plants and is reflected in the composition of the corresponding flyash. When the coal contains 5 percent or more sulfur its elimination in the power plant can be achieved by the introduction of limestone or dolomite in the furnace (14). This affects the composition of the flyash since it will contain calcium or magnesium sulfates.

There are some coals that contain less than 1 percent sulfur and do not require a sulfur removal system. However, since the sulfur content is so low, the resistivity of the flyash (7) is too high for electrostatic precipitators to perform efficiently. In these cases electrolytes,

or sometimes sulfur itself, may be added to raise surface electrical conductivity. These low-sulfur coals are usually CaO-rich and added sulfur under these conditions generates calcium sulfates on the flyashes.

Morphology of Flyash

Flyash particles are predominantly spherical with varying diameters, although it is not unusual to find some angular particles. Natusch et al. (15) classified flyash particles in four groups:

- 1) non-spherical particles which he called "clinkers" and which are characteristically large and light.
- 2) solid spherical particles.
- 3) cenospheres which may be up to 50 μm or larger in diameter.
- 4) plerospheres.

Raask (16) used the term "cenospheres" in 1968 in reference to thin-walled hollow spheres. He discussed the characteristics and formation of these particles which account for up to 5 percent by weight, or up to 20 percent by volume of some flyashes.

"Plerospheres" is a name suggested by Fisher et al. (17) to describe hollow spheres packed with spheres. In the formation of plerospheres Fisher et al. concluded that gas evolution, as an interior process, was a viable explanation. They reported H_2O and CO_2 as the principal gases contained in these spheres, as compared to CO_2 and N_2 reported in cenospheres by Raask.

The color of flyash is variable. Raask and Street (18) considered that the grayness of a flyash depends on the surface area of the black particles in the material. For a

given sample, a reduction in size of the black particles increases the degree of grayness. They did not find a correlation between the appearance or the specific surface of the flyash and its reactivity.

Physical Characteristics

Several workers (19, 20) have tried to find correlations between characteristics such as density, particle size distribution, specific surface and the effects of flyash in concrete. Thorne and Watt (21), and Rehsi (22) considered that the most important physical characteristic of flyash in relation to its activity in concrete is fineness. The amount of flyash passing the 45 μm sieve size is a test referred to by various investigators.

The heterogeneity of flyash is evident in density characteristics as in other parameters. Thorne and Watt (21) separated samples of flyash by density fractions, noting wide variations between samples of different flyashes. They observed that the material in the 2.5 to 2.6 g/cm^3 density range corresponded to clear glass spherical particles. Fractions of higher density included both glassy spheres and a high concentration of crystalline material. Density fractions below this range were mainly spongy textured, glassy particles. Cenospheres were found in the density fraction below 1.0 g/cm^3 .

Raask and Bhaskar (23) also made density fraction separations. Their results represent studies done within specific size fractions. They found that within each size fraction the intrinsic strength of the flyash increased as density increased. Chemical activity of flyash was seen to reach a maximum as density increased while "pozzolanic strength" first increased and then leveled off.

Pozzolanic Reaction

So-called "pozzolanic activity" is controlled by the glass content of the flyash, its particle size, and by the calcium hydroxide available. The reaction between the aluminosilicate glass phase of the flyash and the Ca(OH)_2 provided by the hydration of portland cement is supposed to represent the pozzolanic reaction (24, 25).

When a flyash is used with cement it is usually presumed that the reaction produces a gel in addition to the gel produced through the hydration of cement. Thus, the binding properties are enhanced by the additional gel. Matthews and Gutt (25) and other workers (24) found the reaction products of these pozzolanic reactions to consist mainly of C-S-H tobermorite-like gel very similar to that produced through the hydration of portland cement. They pointed out that the CaO/SiO_2 ratio is lower in the product of the pozzolanic reaction than in the C-S-H product of portland cement hydration. Also noticed was a higher proportion of C-S-H gel in hydrated flyash-cement than in hydrated cement. They considered that this offers an explanation for the enhanced resistance of the flyash concrete to chemical attack through reduced permeability. In this respect Kovacs (24) suggested that secondary phases are responsible for higher strengths at later ages and also provide a denser structure favoring durability.

Minnick (12) proposed that the pozzolanic characteristics of a flyash were due to the stability of the solid phases in the flyash, the degree of subdivision of the flyash particles and their chemical composition. However, he concluded that the crystalline components of flyash do not participate in chemical reactions with calcium hydroxide and water.

In evaluating the pozzolanic activity of flyash both the chemical and physical approaches have been used. Various workers (23, 26) have proposed methods to correlate pozzolanic activity with silica solubility or concentrations of calcium hydroxide. Watt and Thorne (26) made HCl extractions on flyash to determine $(\text{SiO}_2 + \text{Al}_2\text{O}_3 + \text{Fe}_2\text{O}_3)$, and then similar extractions on flyash-lime mortar. They considered the differences obtained an indication of the pozzolanic activity of the flyash. However, they only found good correlation between these chemical analyses and compressive strength up to 6 months. Kokubu (27) considered that the $(\text{SiO}_2 + \text{Al}_2\text{O}_3)$ content of flyash is in close relation to the strength increase of concrete due to pozzolanic reaction.

One of the physical methods that is frequently used to estimate the pozzolanic activity of flyash involves the concept of fineness. The percentage retention on a $45 \mu\text{m}$ sieve is often inversely related to pozzolanic activity. ASTM (9) specifies a maximum of 34 percent to be retained on this sieve. While some workers like Cabrera and Plowman (28) have found no relation between size and strength, several investigators (19, 20, 26, 29, 30) do find correlations. Raask and Bhaskar (23) found that by grinding flyash to different fineness an increase in the pozzolanic activity could be correlated to the square of the specific surface.

Mateos and Davidson (11) worked on the development of an accelerated test to evaluate the pozzolanic activity of a flyash. They mixed 80 percent flyash and 20 percent calcitic hydrated lime to make samples for compression tests. Their work was criticized because their samples were exposed to pressure and temperature conditions different from those normally experienced by flyash concrete.

Effects of Flyash on Concrete

The quality and amount of flyash are determinant factors in the effects of flyash on the strength development of concrete (31). To predict the performance of a flyash concrete it is necessary to specify the quality of flyash to be used or to design according to the known quality. In a concrete mix flyash acts as fine aggregate and as cementitious material, thus it affects all concrete properties (31). Strength, durability, rheological properties of plastic concrete, workability, and cost are some of the aspects influenced by flyash in concrete.

Cabrera and Plowman (28) proposed two types of simultaneous mechanisms to explain the effect of flyash on concrete. The first type is a reduction of water demand without a decrease in workability due to the shape and particle size distribution of the flyash. Related to this is the possibility for better packing of hydration products and unhydrated particles resulting in higher strength and durability.

The second type is chemical in nature and consists of two aspects. One part is the retardation of the hydration of C_3A and C_4AF . In mixes with 30 percent by weight substitution of cement this effect is more pronounced in the case of flyash substitution than if substitution is made with ground quartz. The consequences of this are a lower heat of hydration and a larger volume available for calcium silicates, which will translate into higher strengths. The second aspect of this type of mechanism is the pozzolanic reaction previously discussed.

Kokubu (27), and Matthews and Gutt (25) agree with the first mechanism. Kokubu indicated that reduction in water demand was related to the increasing number of spherical particles with smooth surfaces present as the fineness increases. Kokubu referred to the "finely divided powder

effect" which is also in agreement with the first mechanism proposed by Cabrera and Plowman.

Once the quality of the flyash is recognized and the quality of the cement is considered, the question of what amount of flyash is required arises. Mix proportioning then becomes the most important factor in the properties of the flyash concrete. Berry and Malhotra (32) pointed out three kinds of methods of mix proportioning. One technique consists of replacing part of the cement by flyash. This has the effect of giving lower strengths during the first thirty days, but at later ages strengths are usually higher than those observed on concrete with no replacement. Another possibility is the addition of flyash as fine aggregate with a resultant higher strength of the concrete. A partial replacement of both cement and fine aggregate also gives higher strengths.

It is possible to design flyash concrete mixes that will have equal or higher strengths than normal concretes at any age. Lovewell and Washa (3) concluded that to achieve this at early ages the total weight of portland cement and flyash should be greater than the weight of the cement used in a similar conventional mix. They considered that the actual amounts of flyash depend upon the type of flyash and aggregates used, and on the richness of the mix. At later ages the high strengths that can be achieved with flyash concrete cannot be reached through the use of additional portland cement.

Gosh (33) applied Abram's law to flyash concretes. He related compressive strength, f'_c , to water to cement plus flyash ratio:

$$f'_c = \frac{K_1'}{\left(\frac{W}{C + F} \right)^{K_2'}}$$

K_1' is an empirical constant and K_2' is a constant that depends mostly on the cement properties (34). Use of this relation allows a calculation of the proportion of flyash to cement required for desired results as well as the possibility of estimating the most economic proportion.

Popovics (35) presented other formulas which also relate compressive strength to water to cement plus flyash ratio. He claimed that the new formulas presented in his work would give higher accuracy to proportioning, decrease the number of trial and error batches, and overall favor increased use of flyash in concrete.

Kokubu (36) studied the effects of temperature and curing conditions on flyash concrete. He concluded that cement replacement by flyash not only avoided the negative effect of high temperature on ultimate strength, but at a temperature of approximately 30°C strengths for flyash concrete became higher than those of conventional concretes within a relatively short period. If curing is carried out at low temperatures he found that flyash concrete required moisture for an especially long time to avoid weaker strengths than those of conventional concrete. Kokubu (27) observed that at 3 months or longer the strengths for conventional concretes are lower the higher the curing temperature. For flyash concrete strengths are higher as the curing temperature increases.

Strength and economy are not the only advantages of flyash. In certain cases their inclusion in a mix obeys the desire to obtain greater durability of the concrete. This is especially important when greater impermeability, greater acid and sulfate resistance, or reduced alkali-aggregate reaction are necessary. Work on the permeability of flyash concrete pipe (37) showed that after 28 days curing, flyash concretes were more impermeable than control concretes, and at six months considerable imperviousness

had developed. These results are related to the quantity of hydrated material from cement hydration plus the material resulting from the reaction of the flyash.

Several investigators have made comparisons between the performance of the ASTM class C and class F flyashes in concrete. Usually class C flyashes are compared against class F flyashes because the application of the former to concrete is relatively recent. Dunstan (38) compared flyashes of these two classes in concretes with 15 and 25 percent replacement of cement by weight. He found adequate compressive strength, reduced drying shrinkage, and satisfactory freeze-thaw durability when the ASTM class C was used. However, ASTM class C flyashes drastically reduced resistance to sulfate attack in some cases.

Manz (39) considered that the high lime content of many class C flyashes allows an "internal pozzolanic" reaction. Minnick (40) has observed that when cured in the presence of moisture class C flyashes form complex silicates and sulfoaluminates in a relatively short time. This explains the higher strength values obtained with class C flyashes as compared to class F flyashes.

Heat Evolution

One of the earliest applications of flyash concrete was in massive structures such as dams. The hydration of cement is an exothermic process where the heat evolved may be as high as 100 calories per gram. Temperature rises (34), within mass concrete, of 30°C have been measured allowing for the possibility of temperature differentials (center to surface) in the range of 75°C.

The use of flyash in concrete will reduce the total heat of hydration as well as the rate of heat evolution (25, 34). This behavior is due to the fact that the flyash

reactions are slower than the cement hydration reactions. A consequence of this is a lower compressive strength at early ages but usually a higher strength than conventional concretes at later ages. The percentage reduction in heat evolution at 7 to 28 days is approximately one-half the percentage substitution of cement by flyash.

Flyash and Alkali-Aggregate Reaction

In 1940 Stanton (41) reported that one cause of damage to concrete in the U.S. was aggregate reactivity with cement alkalis resulting in expansion. He found that the addition of finely ground reactive material to the concrete mix could offset this deleterious effect. Since then it has been well established that pozzolanic material has the property of controlling the reaction between cement alkalis and reactive silica aggregates.

Pepper and Mather (42) found that flyash, if used in sufficient amount, prevents excessive expansion. They recommended a 40 to 44 percent by weight replacement of cement as the minimum quantity effective in this sense. They established correlations between effectiveness of the flyash and: fineness, percentage of alkali retained by the reaction product, and dissolved silica.

In explaining alkali-silica reaction, Diamond (43) proposed that the reaction of sulfate ions with calcium aluminates in the cement yields enhanced hydroxide ion concentrations in the pore solution as ettringite precipitates. The equilibrium of a saturated solution of calcium hydroxide is maintained through the dissolution of more calcium hydroxide produced from the hydration of calcium silicates. Chatterji (44) demonstrated that the alkali-silica reaction is controlled by the complete removal of

free Ca(OH)_2 from the concrete, even if an excess of alkali salts or hydroxides is present.

Diamond (45) studied the influence of two flyashes on the alkali contents of cement paste pore solutions. The flyashes had 2.4 and 3.3 percent Na_2O equivalent and some of the alkalies were determined to be "available". Reference cement pastes retained 80 percent of the total potassium and about 60 percent of the total sodium of the cement in solution indefinitely. Pastes prepared with a 30 percent replacement of cement by flyash were found to suffer no contribution from the flyashes toward the alkali content of the pore solution. He observed that one flyash extracted a small proportion of alkalies from the pore solution.

The beneficial action of pozzolans in conjunction with the alkali-aggregate expansive reaction is related by Gutt et al. (46) to an increase in the rate of the reaction in such a manner that it will be over before the cement matrix hardens, or to the complete removal of calcium ions from the pore solution.

CHAPTER 2

MATERIALS USED IN THIS STUDY

Reference Cement

The reference cement used throughout this work was produced by the Lone Star Industries, Inc., Greencastle, Indiana. The chemical composition of this cement is given in Table 2-1. This chemical analysis as well as the flyash chemical analyses were kindly furnished by Martin Marietta Laboratories, Baltimore MD.

Table 2-1. Chemical composition of reference cement.

<u>Oxide</u>	<u>Percent</u>
CaO	64.25
SiO ₂	20.40
Al ₂ O ₃	4.36
Fe ₂ O ₃	2.29
MgO	1.18
Na ₂ O	0.10
K ₂ O	0.76
SO ₃	2.99
TiO ₂	0.24
LOI	2.15

Flyashes

The five different flyashes used in this work will be referred to by a letter name. Table 2-2 shows the source and ASTM classification of each one.

Table 2-2. Source and classification of flyashes.

<u>Flyash</u>	<u>Source</u>	<u>ASTM C 618-80 classification*</u>
A	Muskogee Plant Muskogee, Oklahoma	C
B	Comanche Power Station Pueblo, Colorado	C
C	Otter Tail Power Company Fergus Falls, Minnesota	C
D	Appalachian Power Company Kanawka River Plant	F
E	Appalachian Power Company Clinch River Plant	F

* All flyashes may not meet all requirements of C 618-80.

Flyashes A, B, and C were provided through the courtesy of the power plants concerned. Flyashes D and E were secured through the courtesy of Martin Marietta Laboratories.

Chemical analyses by energy dispersive x-ray spectroscopy, using full ZAF correction, were provided for samples taken from the stock material used in this study. The analyses were converted to oxide form and normalized to 100 percent without the provision for loss on ignition. The results are given in Table 2-3.

Table 2-3. Chemical composition of flyashes, percentage.

Oxide	A	B	C	D	E
CaO	36.9	34.7	30.2	0.9	3.8
SiO ₂	30.1	30.7	30.7	65.0	59.4
Al ₂ O ₃	16.6	15.7	8.2	24.5	21.4
Fe ₂ O ₃	7.0	6.5	8.9	3.9	8.8
MgO	1.4	1.0	2.6	0.0	0.2
Na ₂ O	0.6	1.8	4.1	0.0	0.0
K ₂ O	0.3	0.3	0.9	3.2	4.6
SO ₃	4.4	6.6	12.6	0.0	0.0
TiO ₂	2.7	2.8	1.8	2.5	1.8

These values differ somewhat from the "typical" plant analyses supplied by several of the flyash producers, but are considered to be more reliable. Plant analyses were only obtained for flyashes A, B, and C. The plant analyses gave higher contents of MgO and Al₂O₃ for the three flyashes, but lower contents of CaO.

Some doubt was cast over the high apparent SO₃ content of flyash C. Wet chemical determinations carried out in this laboratory by Mrs. Janet Lovell indicated that only 5.98 percent SO₃ was present in this flyash.

Shortly before this thesis was completed, an entirely new complete wet chemical analysis for this flyash was supplied by Martin Marietta Laboratories. The SO₃ content reported in this analysis was 6.09 percent, in approximate agreement with determinations by Mrs. Lovell. The complete analysis, as supplied by Martin Marietta Laboratories, is given in Appendix A. There are fairly major differences between these results and the energy dispersive x-ray analysis for this material reported in Table 2-3 above.

CHAPTER 3

EXPERIMENTAL METHODS AND TECHNIQUES

The description of the various experimental methods and techniques used in this research are presented in this chapter. In the first part the procedures used for the characterization of the flyash samples are described. The general details of the experimental work with flyash and cement are covered in the second part of the chapter.

The different determinations carried out on the flyashes were done on samples taken from stock material used in this study.

Loss on Ignition

Ignition loss determinations were carried out on all of the flyashes using the procedure of ASTM Method C 311-77 section 11.

Specific Gravity

The determinations of specific gravity of the flyashes were done by the Le Chatelier flask method in accordance with ASTM Method C 311-77 section 20.

Particle Size Distribution

Analyses of the particle size distribution of the flyashes were done by the hydrometer procedure of ASTM Method D 422-63 (Reapproved 1972), normally applied to soil. A four percent NaPO_3 solution was used as a dispersing agent.

X-Ray Diffraction

The x-ray diffraction patterns of the flyashes were obtained using a Siemens D 500 X-Ray Diffractometer. The radiation used was copper $K\alpha$ radiation. The voltage and amperage were consistently set at 50 kV and 20 ma respectively. The slits, going from the x-ray tube to the detector, were arranged in the following manner:
 1° ; 1° ; 1° ; $.15^\circ$; $.15^\circ$.

For each flyash two runs were made, both covering an angular range from 10° to 70° , 2θ . All samples were run at an angular speed of 1° 2θ per minute. The first run was made with a 2-second time constant, setting the recorder at 2 cm/min., in order to obtain a good resolution for identification of the peaks. The second run was made with a 4-second time constant, and a recorder speed of 1 cm/min., in order to have a better presentation of the patterns, since the first run patterns showed much hashiness.

The samples for each x-ray run were prepared as random powder mounts. Each sample was ground in a mechanical pulverizer ("Wig-L-Bug", Spex Instruments, Inc), used for reducing small samples for analysis. Each sample was passed through a No. 100 (150 mm) sieve into a rough-textured piece of paper in the sample mount arrangement. The paper

was subsequently removed, uncovering the surface to be exposed to the x-ray beam. This technique, designed to avoid preferential orientation, is known as the modified McCreery mount method.

Semiquantitative Analysis by Energy Dispersive X-Ray Analysis

These analyses were obtained using an ISI Super III A scanning electron microscope and an EEDS II Energy Dispersive X-Ray Analyzer (E. G. and G. Ortec Co., Inc.). An accelerating voltage of 30 kV was consistently used in the scanning electron microscope (SEM).

The preparation of the samples was done on a 25 mm diameter SPI porous silver membrane mount with a pore diameter of nominally 0.45 μm . The silver membrane was placed on the porous glass support of a Millipore filtering outfit. A glass cylinder was fixed with a clamp on top of the silver membrane, filled with acetone, and a small amount of flyash was introduced. The filter apparatus was agitated and mounted over a Buchner flask and a slight vacuum was applied to induce passage of the suspension and deposition of a layer of the flyash on the surface of the silver membrane. The silver membrane with the sample was then glued on to an SEM sample stub with silver paste, and the sample lightly coated with a gold-palladium alloy using a sputter type coater (Technics Hummer I). The coating was carried out for two minutes at 150 millitorr, with the current set at 10 amp and the voltage at 11 V.

Spheres were chosen for analysis that fell in the following size ranges:

- a) $1 \mu\text{m} < d < 5 \mu\text{m}$
- b) $5 \mu\text{m} < d < 10 \mu\text{m}$
- c) $10 \mu\text{m} < d < 15 \mu\text{m}$
- d) $15 \mu\text{m} < d < 20 \mu\text{m}$
- e) $d > 20 \mu\text{m}$

On each sphere spot analyses were carried out with the beam held stationary in each of three spots: a spot on the center; a spot left of the center; and a spot right of the center. On most particles a rastered surface analysis was also performed. The image observed on the SEM screen was magnified sufficiently to make the particle cover the screen, and then the counts were acquired by the EDXA. In selecting spots for analysis each sphere was considered to be divided into three slices by two vertical planes, each spaced $1/6$ of a diameter's distance left and right of the center. Representative spots were selected on the upper portion of each of the three slices, and these were designated left, center, and right, respectively. The geometry is sketched in Figure 3-1.

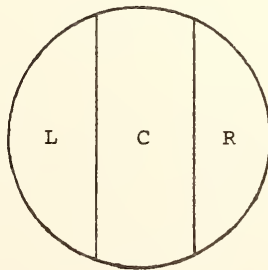


Fig. 3-1. Scheme for selecting spots for analysis on flyash spheres.

A "region of influence" for the x-ray peak of each element of interest was laid out around its K peak on the EDXA screen so as to avoid overlapping, as follows:

Na	0.96	-	1.12	keV
Mg	1.14	-	1.32	"
Al	1.36	-	1.58	"
Si	1.62	-	1.86	"
K	3.20	-	3.42	"
Ca	3.56	-	3.80	"
Ti	4.36	-	4.64	"
Fe	6.24	-	6.54	"

The time set for acquiring counts was 100 seconds live time for each determination.

All of the cement-flyash systems studied in this work were prepared from mixes in which 30 percent of the weight of the cement in reference portland cement systems was replaced by the same weight of flyash. A constant 0.5 water to cement ratio was used for the reference portland cement systems, and a constant 0.5 water to solids ratio was used for the cement-flyash systems; the solids being cement plus flyash. These common characteristics were maintained in paste mixes, mortar mixes, and concrete mixes. Deionized water was used in all paste and mortar mixes.

Pastes were cast in rigid plastic "ointment jars" of 5.1 cm diameter and 6.5 cm height. These are nominally 4 oz jars, and have a volume of approximately 120 ml. These plastic containers were used for determinations of setting time, for heat evolution, and for expression of pore solutions.

Mixing Procedure for Pastes

Paste mixing was done according to ASTM Method C 305-80 for mechanical mixing of hydraulic cement pastes. Previous to the contact of solids and water, the cement and flyash were hand mixed using a rubber spatula.

Setting Time

The time of setting of the pastes under study was determined with a Vicat needle apparatus. The paste was poured into the plastic container, in one single layer, to about 2.0 mm below the height of the container. The cap of the container was screwed on and only for testing was it taken off. The container remained in the laboratory during the testing and waiting periods. The criteria and procedure for determining the initial and final set complied with ASTM Method C 191-79 section 6.2.

Temperature Evolution

To measure the temperature evolution of the pastes during hydration a device designed by Professor D. N. Winslow was used. This consisted of a two piece (base and lid) styro-foam insulating block with a carved out space for two snugly fitting plastic ointment jars as described previously. These are sufficiently separated in the insulating block so as to avoid heat transfer between them.

The caps of the containers have a 1/2 inch central hole drilled through them to allow copper tubes to be passed through them. One end of a copper tube is crimped shut and positioned roughly midway through the hydrating paste. Ducts

bored through the styrofoam allow the insertion of a thermistor into each plastic container and into the copper tube. A few milliliters of mercury poured in the copper tubes provide thermal contact between the copper tube and the thermistor. The thermistors are connected to a Wheatstone bridge, the output of which is fed into a strip-chart recorder.

One of the containers was used for the paste under study and the other one was used for the reference material. Ottawa sand ("C 109 sand") and water, with a water to sand ratio of 0.5 was used as the reference. Immediately after mixing, the paste was cast in one single layer in the plastic container, sealed, and placed in the styrofoam block base; the lid was then fixed on, isolating the system. The crimped ends of the copper tubes were embedded in the reference material and in the paste.

Expression of Pore Solution from Pastes

Once mixed, the pastes were cast in one single layer in the plastic ointment jars. These were vibrated 30 s at "50" on a Syntron Joggèr vibrating table. The plastic containers were covered with "parafilm" plastic sheeting before screwing the cap on.

Two methods for obtaining the pore solutions were employed. For hydration periods less than the time of the initial set, a Millipore pressure filtering system was used. Specimens six hours old or more were instead subjected to high pressure (from a hydraulic loading machine) in a special steel die apparatus to literally "squeeze out" the pore solution.

The Millipore filtering system used nitrogen gas from a cylinder as the source of pressure. Filtering membranes of 0.8 μm pore size and 47 mm diameter were placed in this apparatus, the paste added, and pressure applied. A diagram of the set up is shown in Figure 3-2.

The pore solution expression apparatus for set pastes consists of a cylindrical steel die with a concentric bore for the insertion of a steel piston. This rests on top of a steel platen provided with a drain ring in its top so as to collect and direct the pore solution through a fluid channel to a collecting syringe. Heavy plastic tubing is used as a connection between the platen and the syringe. Figure 3-3 shows an isometric half-section of this apparatus.

Before each use all the bearing surfaces of the apparatus were cleaned with ethanol and allowed to dry. A coating of film bonding grade fluorocarbon was sprayed on interacting surfaces. The die was placed on the center of the platen and the sample placed in the bore. A tightly fitting teflon disc was inserted over the sample and the piston introduced into the bore above it.

The apparatus was then centered under the loading plate of a Forney Testing Machine (Model No. FT 40 DR). The plastic tubing was inserted into the drain channel and a syringe fitted to it. Load was slowly applied till the pore solution was obtained, with 200,000 lbf being the limiting load for safety reasons. Especially with pastes over a month old, it is convenient to reach the maximum stress level and maintain the load for a few minutes, and then reduce the pressure to allow some elastic rebound to occur. The pressure is then increased back to the maximum level and additional pore solution can be withdrawn.

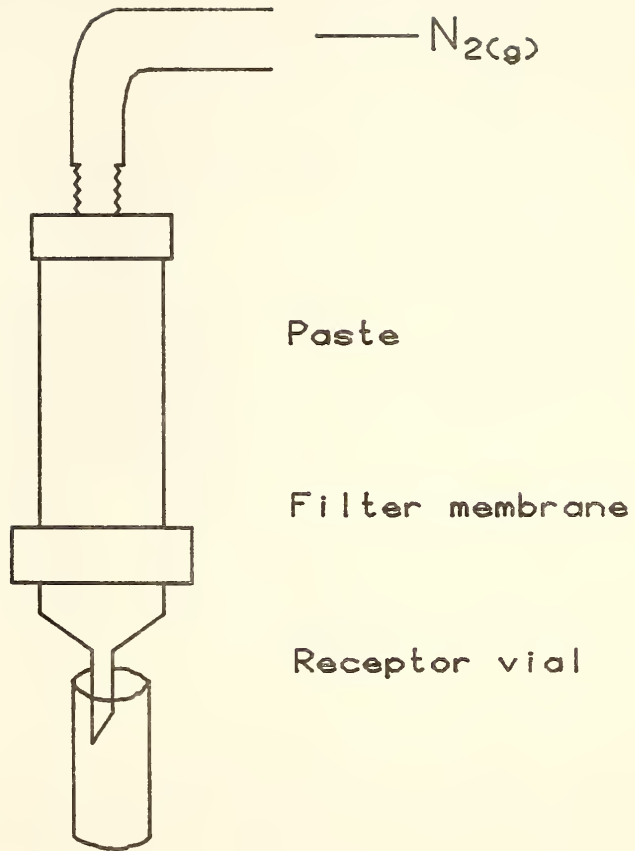


Fig. 3-2. Millipore pressure filtering system used to obtain pore solution from cement pastes.

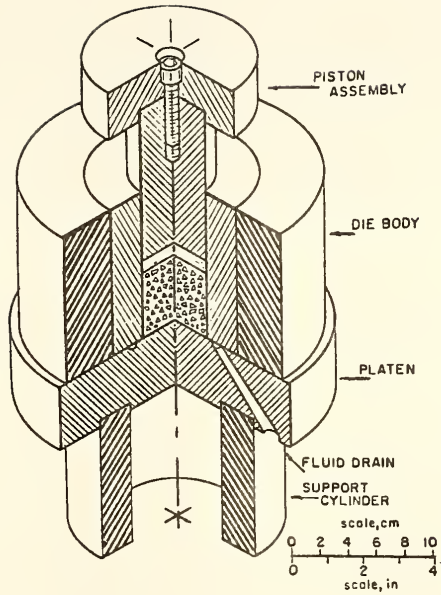


Fig. 3-3. Isometric half-section of the pore solution expression apparatus (47).

Non-Evaporable Water Determinations

After the expression of the pore solution a portion of the compressed paste was immediately immersed in acetone to stop the hydration process. Excess acetone was poured out and this portion of the sample was left in the oven drying overnight at 1050°C. Approximately 5 g portions of the sample were weighed in porcelain crucibles and placed in the muffle furnace overnight at 1050°C. The weight difference due to the muffle furnace treatment represents the loss on ignition, which after correction for LOI of the starting materials provides a measure of the amount of non-evaporable water.

Chemical Analyses of Pore Solutions

The concentrations of the following ions were determined on all pore solutions: OH^- , $\text{SO}_4^{=}$, Ca^{2+} , Na^+ , and K^+ . Hydroxide ion concentration was determined with HCl; concentrations of all other ions were determined with a Perkin-Elmer 503 Atomic Absorption spectrophotometer.

Immediately after obtaining the pore solution a 1 ml (0.5 ml for older pastes) aliquot was titrated with HCl (0.05 N) using methyl red as indicator. The HCl was standardized against 0.2 N Na_2CO_3 .

Immediately after this determination was completed, a second 1 ml aliquot of the pore solution was placed in a 100 ml volumetric flask. Two milliliters of a 50,000 $\mu\text{g/ml}$ La^{3+} solution were added to the flask, as well as 2 drops of concentrated HCl. This was diluted to the mark with deionized water and shaken vigorously. This 100 X diluted pore solution was the stock solution for all the other determinations.

Calcium was determined in the atomic absorption mode of the spectrophotometer. The conditions set for this determination were: wavelength - 422.7 nm; slit - 4; elevation of the burner - 4.8. A lean N_2O -acetylene flame was used.

The determination of potassium was done in the flame emission mode. The working conditions in this case were: wavelength - 383.5 nm; slit - 4; filter; chopper; elevation of the burner - 2.0. Even though these determinations were carried out with a lean air-acetylene flame, the nitrous oxide burner (placed at 30° to the beam path) was used.

In determining sodium the flame emission mode was used. The conditions for these determinations were: wavelength - 294.7 nm; slit - 3; chopper; elevation of the burner - 2.0. As in the potassium determinations, a lean air-acetylene flame and the nitrous oxide burner (at 30° to the beam path) were used for sodium determinations.

Sulfate determinations were done following an indirect method. To 40 ml stock pore solution 40 ml of a 200 g/ml $BaCl_2$ solution, 4 ml of a 5 percent KCl solution, and four drops of concentrated HCl were added. This was diluted to 100 ml and agitated vigorously, then allowed to rest overnight. Sulfate was then quantified by determining the excess barium after the reaction that precipitated sulfate as $BaSO_4$. These determinations were carried out in the flame emission mode. The conditions were: wavelength - 277 nm; slit - 2; chopper; elevation of the burner - 2.0. A rich nitrous oxide-acetylene flame was used.

Mixing Procedure for Mortar and Preparation of Mortar Cubes

The mixing was done according to ASTM Method C 305-80 for mechanical mixing of hydraulic cement pastes and mortars of plastic consistency. Prior to the initial contact of solids and water, the cement and flyash were hand mixed with a rubber spatula. Two-inch cubes were cast in accordance with ASTM Method C 109-80. The mortar cubes were demolded at one day and stored immersed in saturated limewater up to the time of testing.

Compressive Strength Tests of Mortar Cubes

The compressive strength tests were run using a Forney Hydraulic Testing Machine model FT 40 DR. The samples were not allowed to dry prior to testing.

Mixing Procedure for Mortar and Preparation of Mortar Bars

These mixes had a four percent by weight substitution of the sand by reactive silica in the form of ground Beltane opal. The mixing was done following the procedure of ASTM Method C 305-80. Prior to the first contact of solids and water the cement and flyash were hand mixed with a rubber spatula; likewise the sand and beltane opal were also hand mixed with a rubber spatula. The bars were molded according to ASTM Method C 157-75 section 5 and ASTM Method C 490-77.

Storage and Observation of Length Changes in Mortar Bars

Demolded after 24 hours, the bars were permanently stored in sealed boxes in a constant temperature, constant humidity room set at 23°C and 50 percent relative humidity. Plastic shoe boxes, lined in their inner sides with blotting paper, were used as containers. The liner extended into the water in the bottom of the container and above the top of the bars. The four specimens that fit into each box rested horizontally on two glass rods perpendicular to the bars. The water level was always maintained such that it would not cover the glass rods. Each box held the bars corresponding to each one of the mixes.

The length comparator used for measuring length changes of specimens has a high-grade micrometer graduated to read in 0.0001 inch units. The reference bar used as a standard for the gage dial setting has an overall length of 11 5/8 in.

Mix Design for Concrete and Casting of 3 X 6 in Cylinders

All of the concrete cylinders for this study were cast during one session. The mix designs were made following the ACI Standard: Recommended Practice for Selecting Proportions for Normal Weight Concrete (ACI 211.1-70).

The coarse aggregate used was a locally available crushed limestone; the fine aggregate was a heterogeneous natural sand. The maximum size of coarse aggregate, CA, was set at 3/4 in. The specific gravity of the CA was found to be 2.6 and its dry rodded weight was 104 lb/ft³. The fineness modulus of the sand, FA, was 2.8 and its specific gravity was 2.7

These parameters, as well as those pre-established at the beginning of this chapter gave rise to the mix designs shown in Table 3-1.

Table 3-1. Mix designs for cement-flyash concrete systems and reference concrete.

<u>Materials</u>	<u>SYSTEM</u>		
	<u>A, B, and C</u> <u>lbs</u>	<u>D and E</u> <u>lbs</u>	<u>Reference</u> <u>lbs</u>
Cement	28.6	28.6	40.8
Flyash	12.2	12.2	----
FA	67.2	65.9	68.9
CA	104.5	104.5	104.5
Water	20.4	20.4	20.4

All of these concrete mixes were mixed by hand using a trowel and a mixing pan. ASTM Method C 192-76 section 5.1.3 was followed in this respect. The cylinders were cast in three layers consolidating with a rod; each layer received twenty strokes. The specimens were left covered with plastic during 24 hours and then demolded and placed in a fog room.

Compressive Strength Tests of Concrete Cylinders

ASTM Method C 39-72 (Reapproved 1979) was followed to determine the compressive strength of the concrete.

CHAPTER 4

RESULTS AND DISCUSSION

The format of this chapter is similar to that of chapter 3, in that it is divided into two main parts. Characterization of the flyash samples is covered in the first part, and the results for the experiments with pastes, mortar, and concrete are given on the second part.

Loss on Ignition

The results of ignition loss determinations, carried out in duplicate on each of the flyashes, are given in Table 4-1. Loss on ignition reflects both the carbon and any carbonate content of a flyash. In these flyashes the ignition losses are all less than two percent, indicating excellent burning in all of the power plants concerned.

Specific Gravity

Table 4-2 shows the results of the specific gravity determinations carried out in duplicate on each of the flyashes. It is observed that the class C flyashes show distinctly higher specific gravities than the class F flyashes. The difference is significant, amounting to almost 20 percent.

Table 4-1. Ignition loss determinations of flyashes.

<u>Flyash</u>	<u>ASTM Class</u>	<u>Percent</u>
A	C	1.22
B	C	1.94
C	C	1.65
D	F	1.67
E	F	1.00

Table 4-2. Measured values of specific gravity of flyashes.

<u>Flyash</u>	<u>ASTM Class</u>	<u>Measured specific gravity</u>
A	C	2.58
B	C	2.63
C	C	2.81
D	F	2.17
E	F	2.15

Particle Size Distributions

The cumulative particle size distribution curves determined for the five flyashes are shown in Figures 4-1 and 4-2. The three class C flyashes are represented in the first figure and the two class F flyashes are shown in the second figure. The data were obtained by successive hydrometer readings, a total of 14 readings being made for each determination. The usual continuous plot of particle size distribution was then prepared. Because of extensive overlapping between the individual flyash distributions, Figures 4-1 and 4-2, which represent continuous curves, are shown only discontinuously with the points spaced so as to minimize overlap and confusion.

A further indication of the size distributions and how they compare with each other is provided in the data of Table 4-3, which lists the diameters corresponding to the 75, 50, and 25 weight percentiles. The size range seems to be almost entirely between 50 μm and 1 μm .

Table 4-3. Stated percentile diameters representing the size distributions of the flyashes, μm .

<u>Percentiles, finer than</u>	<u>A</u>	<u>B</u>	<u>C</u>	<u>D</u>	<u>E</u>
75 %	35.0	25.5	29.5	31.5	28.0
50 %	13.5	12.0	13.0	20.0	13.0
25 %	3.3	3.5	4.2	11.5	5.8

Flyash D seems substantially coarser than the others. This flyash has a weight mean (50th percentile) diameter of 20 μm ; the weight mean diameter of all of the other flyashes is between 12 and 14 μm . Flyashes A, B, C, and E have particle size distributions that are all quite similar to each other.

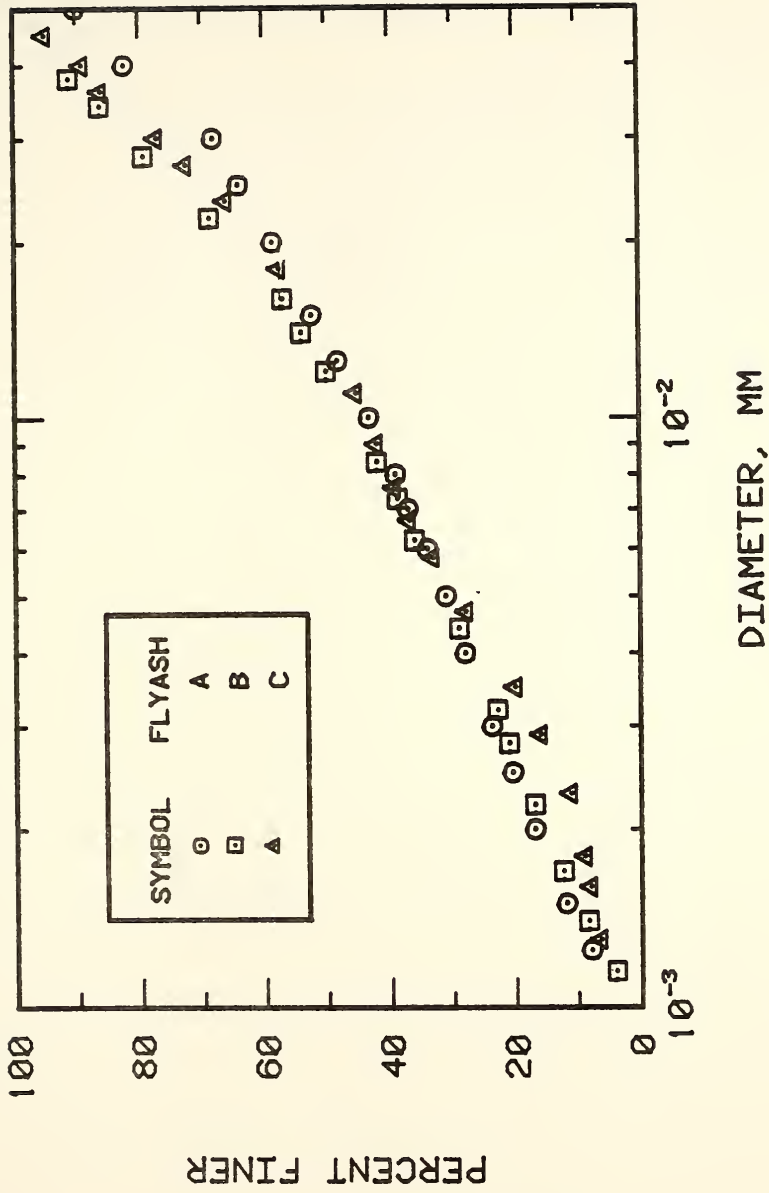


Fig. 4-1. Particle size distribution of flyashes A, B, and C.

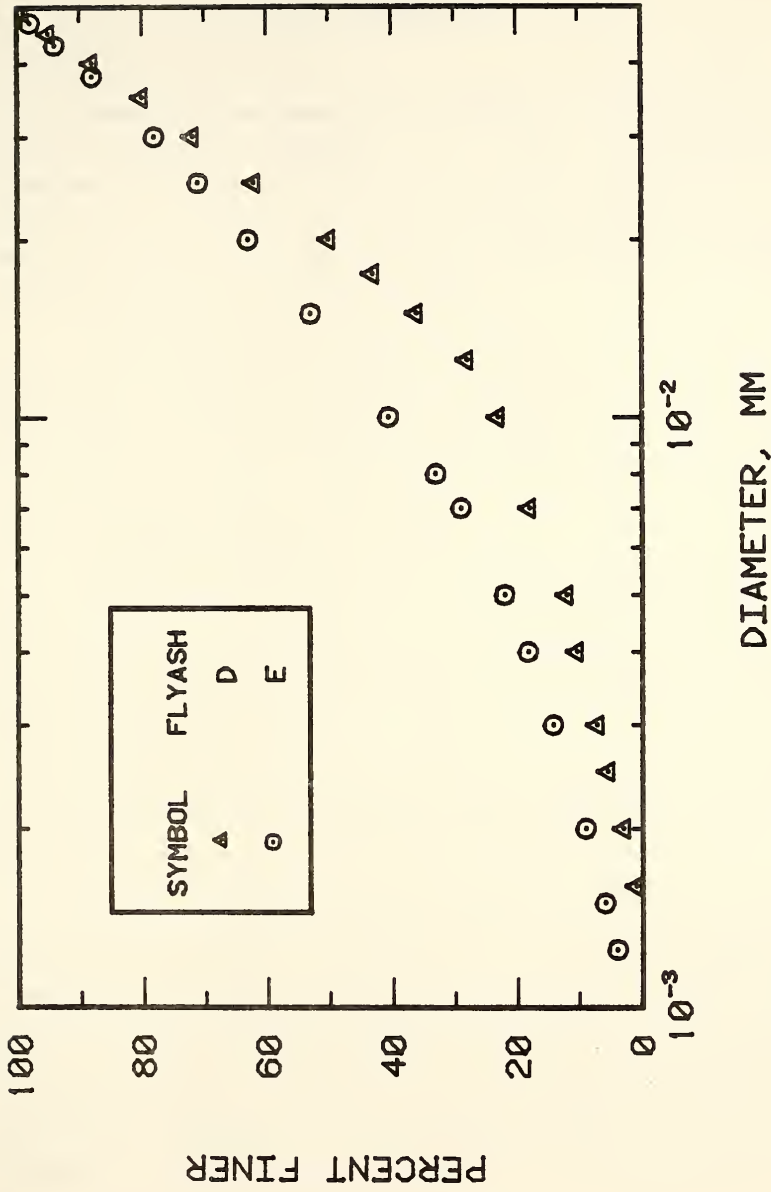


Fig. 4-2. Particle size distribution of flyashes D and E.

X-Ray Diffraction

X-ray diffraction patterns were secured for each of the flyashes and are shown in Appendix A. Interpretation of the patterns of flyashes A, B, and C, the high-lime flyashes, is complex because of the large number of compounds present. In contrast the low-lime flyashes, D and E, have only a few crystalline components and interpretation is fairly straightforward.

The only constituent common to all of the flyashes is quartz, with hematite present in all but flyash A. In addition the low-lime flyashes (D and E) both contain mullite and brookite. The three high-lime flyashes show anhydrite in addition to quartz. Two of these ASTM class C flyashes, B and C, also have alkali sulfates in various forms as well as crystalline calcium oxide.

The components identified in these flyashes are indicated as either confirmed (those for whose identification there is sufficient evidence) or as probable components. In the last category are included those reasonable components whose diffraction pattern is recognizable, but that show considerable overlap of their peaks with other peaks in the patterns. Looking only at the confirmed components it is not so obvious that the high-lime flyashes are more complex, but it is considering the probable components that the difference is clear.

A list of the components identified in each of the flyashes is provided in Table 4-4. In this table the mineral name as well as the formula are given for each component. The numbers shown are the x-ray powder diffraction file numbers given by the Joint Committee on Powder Diffraction Standards to the compounds concerned. A plus sign indicates a confirmed presence, a negative sign indicates an absence, and a P stands for a probable presence.

Hillebrandite and calcio-chondrodite are highly suspected (HS) compounds in flyash A and C, but their presence was not confirmed. These are hydrated compounds whose identification in flyash may be questionable.

Sulfates are conspicuously present in the high-lime flyashes. The presence of calcium aluminate sulfate ($C_4A_3\bar{S}$) and aphytholite ($(Na, K)\bar{S}$), confirmed in flyash A, is probable in flyashes B and C. α - K_2SO_4 was confirmed in flyash C.

The occurrence of aluminum compounds in flyashes A, B, and C is larger than in flyashes D and E. The presence of calcium aluminate (C_3A) was confirmed in flyashes A and B, and its presence in flyash C was considered probable. Gehlenite (C_2A_2S) and mullite (A_3S_2) were both confirmed in flyash B and their presence is probable in flyash C. Kappa-alumina was confirmed in flyashes B and D, probably found in flyashes A and C, and absent in flyash E.

Titanium compounds were only confirmed in the ASTM class F flyashes. However, their presence was considered probable in the high-lime flyashes, especially flyashes B and C. The presence of brookite (TiO_2) was confirmed in flyashes D and E. In flyash D the presence of perovskite ($CaTiO_3$) and pseudorutile ($Fe_2Ti_3O_9$) were confirmed.

The difference between the ASTM class C and class F flyashes used in this study, with respect to their x-ray diffraction patterns, resides in the major crystalline components found in them. Not considering quartz, which is the major component in all five flyashes, the high-lime flyashes are characterized by the presence of crystalline calcium oxide, anhydrite, and calcium aluminate (C_3A). Flyashes D and E are characterized by the presence of mullite as a major component.

Table 4-4. Crystalline components identified in the flyashes.

Component	A	B	C	D	E
Alpha quartz					
SiO ₂ 5-490	+	+	+	+	+
Crystalline calcium oxide					
CaO 4-777	P	+	+	-	-
Anhydrite					
CaSO ₄ 6-226	+	+	+	-	-
Soluble anhydrite					
γ-CaSO ₄ 2-134	-	-	+	-	-
Calcite					
CaCO ₃ 5-586	+	-	+	-	-
Tricalcium silicate					
C ₃ S 11-593	+	+	P	-	-
Calcium aluminate					
C ₃ A 8-5	+	+	P	-	-
Calcium aluminate sulfate					
C ₄ A ₃ S̄ 16-335	+	P	P	-	-

Table 4-4, continued.

Component	A	B	C	D	E
Gehlenite					
C_2A_2S 9-216	-	+	P	-	-
Mullite					
A_3S_2 15-776	-	+	P	+	+
Thenardite					
Na_2SO_4 5-631	-	+	+	-	-
Meta-thenardite					
Na_2SO_4 form I 1-990	-	-	P	-	-
$\alpha-K\bar{S}$					
K_2SO_4 3-565	-	-	+	-	-
Aphthitolite					
$(Na, K)\bar{S}$ 1-978	+	P	P	-	-
Kappa-alumina					
$K-Al_2O_3$ 4-878	P	+	P	+	-
Periclase					
MgO 4-829	P	+	P	-	-

Table 4-4, continued.

Component	A	B	C	D	E
Hematite					
Fe ₂ O ₃ 13-534	-	+	+	+	+
Magnetite					
Fe ₃ O ₄ 11-614	P	P	+	+	P
Anatase					
TiO ₂ 4-477	-	P	P	P	P
Brookite					
TiO ₂ 16-617	-	P	P	+	+
Rutile					
TiO ₂ 4-551	-	P	-	P	P
Perovskite					
CaTiO ₃ 8-91	-	-	P	+	-
Pseudobrookite					
Fe ₂ TiO ₅ 9-182	P	-	P	-	P
Pseudorutile					
Fe ₂ Ti ₃ O ₉ 19-635	-	P	P	+	P

Table 4-4, continued.

Component	A	B	C	D	E
Kalsilite					
KAlSiO ₄ 3-540	-	P	+	-	-
Hillebrandite					
C ₂ SH 11-594	HS*	-	HS	-	-
Calcio-chondrodite					
C ₅ S ₂ H 11-300	HS	-	-	-	-

* HS indicates that the component is highly suspected.

In addition to the peaks for the crystalline components, a background "hump" is indicative of the substantial content of glass present in each of the flyashes. As indicated in Figure 4-3, the high-lime flyashes show a smaller "hump", which is asymmetric and displays a maximum at 33° 2θ. In contrast the low-lime flyashes show significantly larger "humps" with maxima at 23° to 24° 2θ. The "humps" on flyashes D and E are taller than those of the high-lime flyashes by factors of 1.5 and 2.1 respectively. The difference in the position of maxima for these "humps" undoubtedly reflects differences in the chemical composition of the glass present.

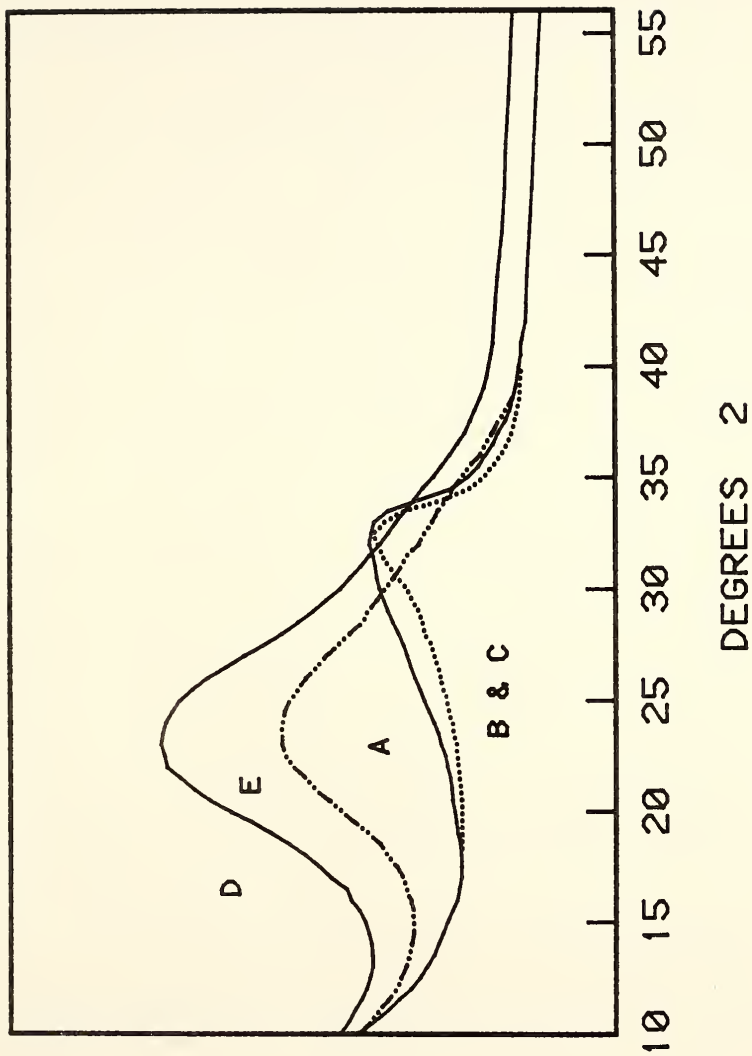


Fig. 4-3. Effect of glass content on the x-ray pattern of each flyash studied.

Semiquantitative Analysis by Energy Dispersive X-Ray Analysis

Energy dispersive x-ray analysis (EDXA) was used to examine the compositions of individual flyash particles under observation in the SEM. An attempt was made to study the variation in chemical composition of the flyashes as a function of particle size. For each size range about twelve particles (sometimes more) were chosen for analysis in flyashes A and D, and about eight in flyash B. Because of the time-consuming nature of these studies they were carried out only on flyashes A, B, and D.

The data obtained showed good concordance among the three spot analyses and the rastered surface analysis done on each particle. The graphical representation of all of the large numbers of analyses carried out is cumbersome in the extreme and difficult to assimilate. However, after much effort a condensed form of representation was developed and is shown in Figures 4-4 thru 4-6.

Each analysis yielded a measured ratio of the peak area of the element concerned to the peak area of the silicon peak of the flyash particle being examined. A logarithmic scale is used to display the ratio values of each element to silicon. Silicon appears in the composition of all particles and would be represented in all analyses by a horizontal line at a peak area ratio value of 1.00. For each other element there are five vertical lines corresponding to each of the five size ranges. The order of these lines, going from left to right, corresponds to the size ranges in increasing order, viz., 1 - 5 μm , 5 - 10 μm , 10 - 15 μm , 15 - 20 μm , and 20 μm .

The spread of each vertical line over the ratio values scale represents the full actual dispersion in the ratios observed. The circle represents the mean of all the values represented by each line. In some cases the vertical

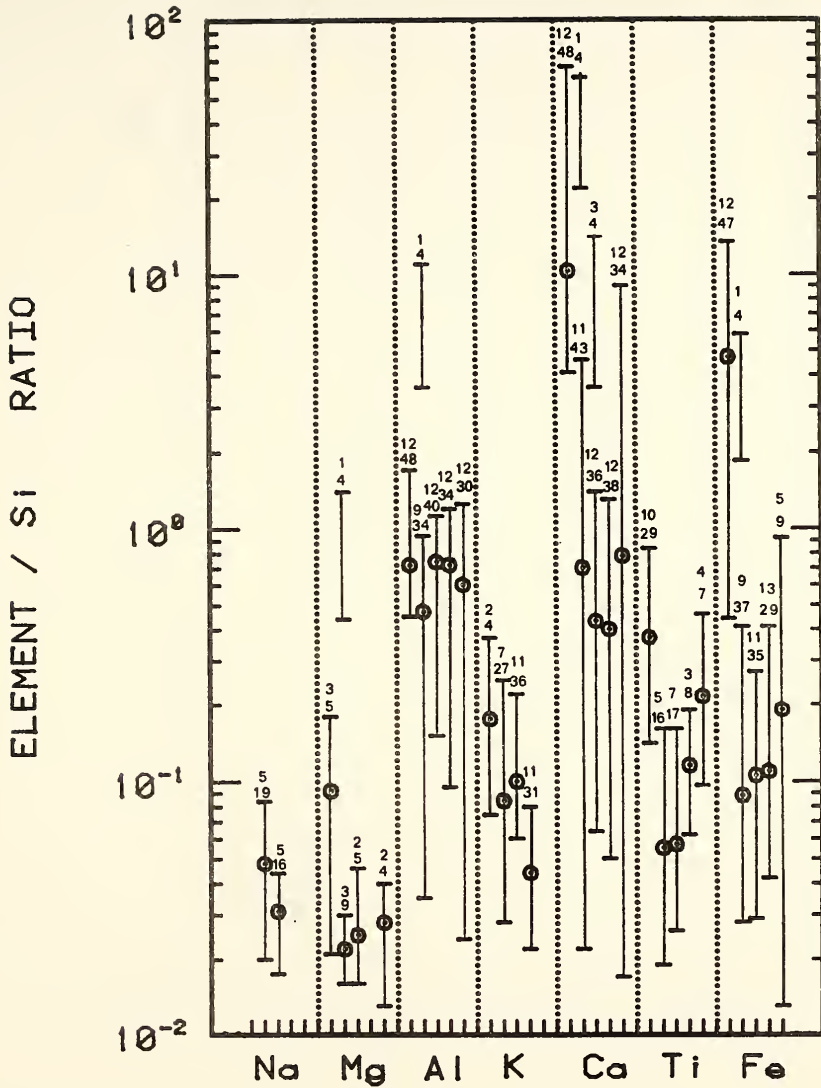


Fig. 4-4. Semiquantitative peak intensity ratio of elements to silicon in flyash A.

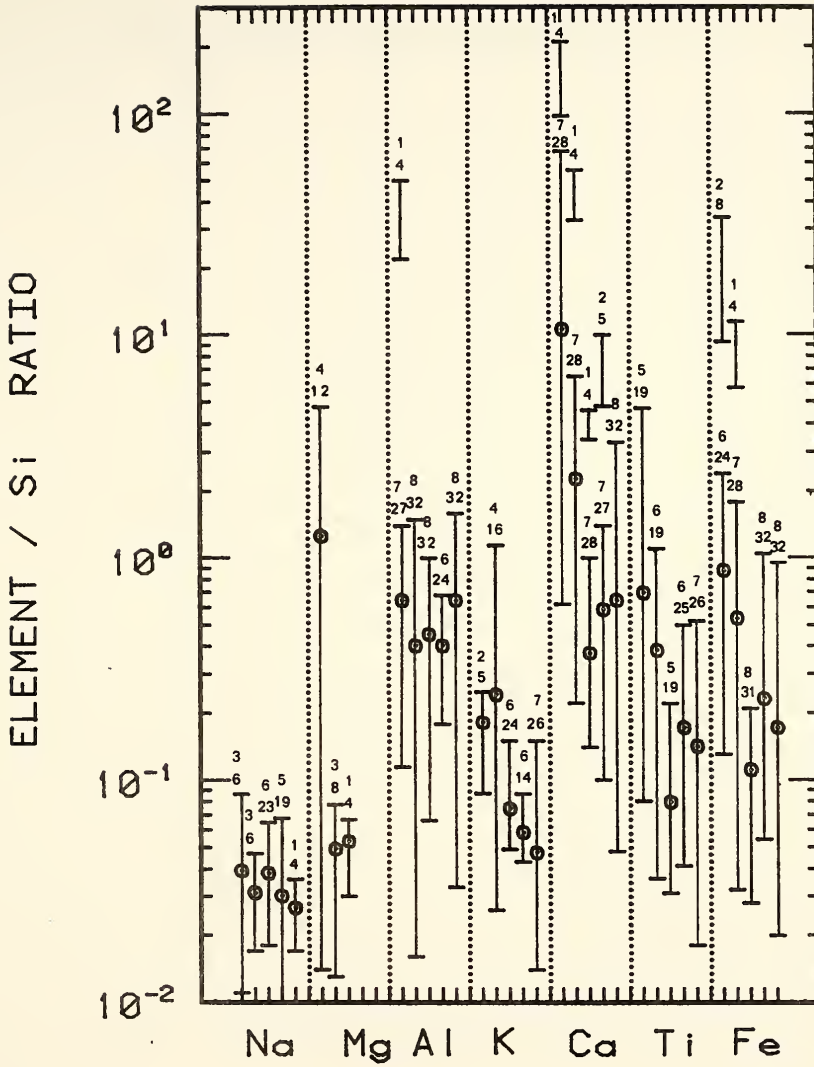


Fig. 4-5. Semiquantitative peak intensity ratio of elements to silicon in flyash B.

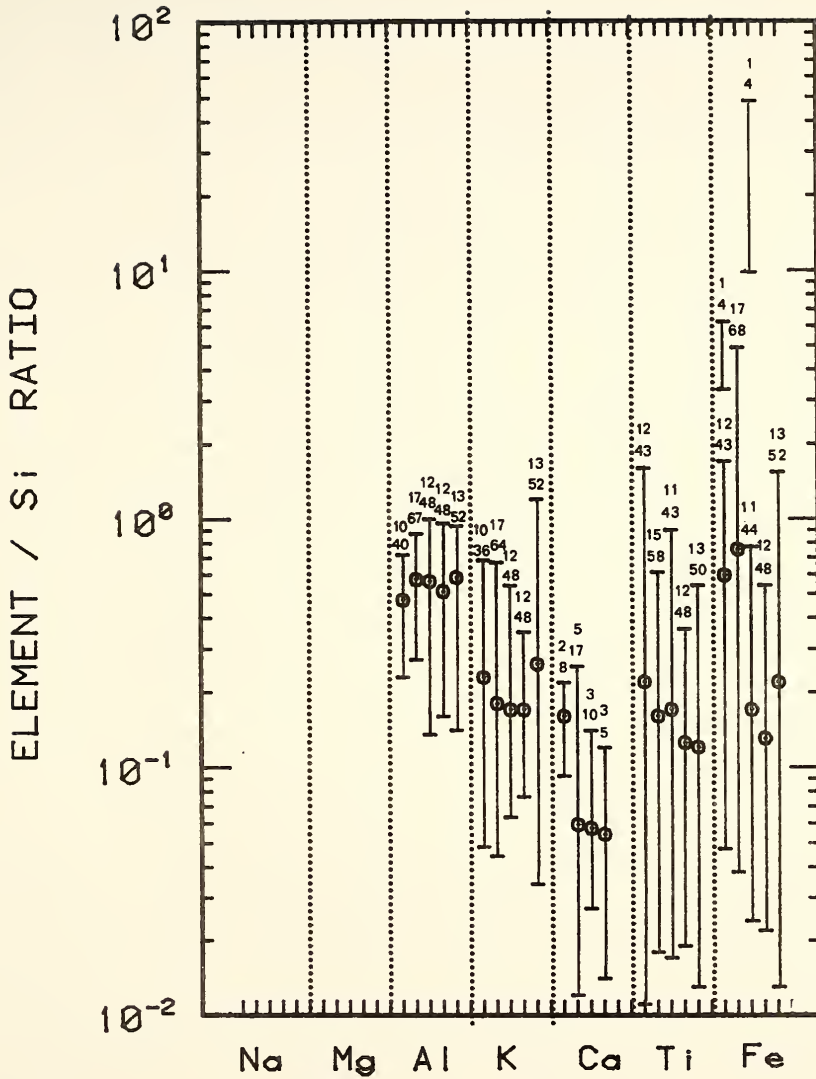


Fig. 4-6. Semiquantitative peak intensity ratio of elements to silicon in flyash D.

lines are broken; the gaps represent an extensive intermediate range of values not found in the particles. There are two numbers above each vertical line representing a size range. The upper number is the number of particles of the set that contain the element in question. The lower number is the total number of individual analyses represented in the vertical line.

For simplicity a few individual analyses which are atypically outside the range for the element concerned are not plotted. These number 31 analyses out of a total of over 800 for flyash A, and only 3 and 2 respectively for flyashes B and D.

From Figures 4-4 thru 4-6 it is observed that there seems to be a general dependence of the chemical composition of the flyash on the particle size. This is not shown for aluminum, the aluminum to silicon ratio being virtually constant for a given flyash throughout all the size ranges. In all three flyashes it is seen that the smallest particles show ratios, of most elements to silicon, that are higher than for the other particles. This is observed mostly with the 1 - 5 μm particles, although sometimes the 5 - 10 μm particles show the highest ratios.

In flyashes A and B the ratios of Mg, K, Ca, Ti, and Fe to silicon for the 1 - 5 μm particles are anywhere from about two to about twenty times as high as the corresponding ratios for the larger particles. This tendency is not as evident with the class F flyash, flyash D, but even here the ratios for Ca, Fe, and Ti to silicon are two or three times higher for the fine particles. However, it must be pointed out that flyash D has a 65 percent content of SiO_2 whereas flyashes A and B have approximately 30 percent SiO_2 . This could be an important factor in the attenuation of the effect in flyash D. From these observations it is inferred that the 1 - 5 μm

particles have a proportionately lower content of silicon than the larger particles in each of these three flyashes.

The elemental composition of these flyashes can be divided into major and minor elements. The ASTM class C flyashes have silicon, aluminum, and calcium as the major elements and Na, Mg, S, K, Ti, and Fe as the minor elements. The ASTM class F flyashes have silicon and aluminum as the major elements and Ca, K, Ti, and Fe as the minor elements, with a small amount of Mg in flyash E.

Comparing this observation of the composition of the high-lime flyashes to the results obtained from the EDXA, it is found that the ratio of the minor elements to silicon is usually less than 1.0 for the particles greater than 5 μm . The mean ratio values of these elements to silicon is less than or about 0.2. In the low-lime flyash, flyash D, the ratio of the minor elements to silicon is usually less than 1.0 for particles greater than 5 μm . The mean ratio value of these elements to silicon is less than or about 0.25. Thus the relationships of the minor elements to silicon is very similar in the three flyashes.

For the major elements aluminum has been discussed previously. In the ASTM class C flyashes calcium appears in the 1 - 5 μm particles overwhelmingly accounting for the greatest part of the composition. Ratio values of calcium to silicon greater than one and up to seventy are observed in this size range. In the 1 - 5 μm particles of flyash A the iron peak, on the average, is five times more intense than the silicon peak.

The mean ratio values for each flyash are tabulated in Tables 4-5 thru 4-7. For each size range the percentage of particles is shown as obtained from the particle size distribution plots of Figures 4-1 and 4-2. For each element a summation of the products of the mean ratio

Table 4-5. Weighted mean peak intensity ratio of each element to silicon in flyash A as compared to the corresponding overall ratio.

Element	Mean ratios of each element to silicon in each of the following size ranges given in μm . Shown also are the percentages of particles in each size range.						Weighted mean ratio	Overall ratio
	1 - 5 31.0	5 - 10 12.0	10 - 15 9.5	15 - 20 6.0	> 20 41.5			
Na	0.00	0.05	0.03	0.00	0.00	0.00	0.01	0.02
Mg	0.09	0.02	0.03	0.00	0.03	0.03	0.05	0.06
Al	0.73	0.48	0.72	0.71	0.60	0.60	0.64	0.31
K	0.18	0.08	0.10	0.04	0.00	0.00	0.08	0.01
Ca	10.42	0.72	0.43	0.40	0.79	0.79	3.71	1.87
Ti	0.38	0.05	0.06	0.11	0.22	0.22	0.22	0.12
Fe	4.73	0.09	0.10	0.11	0.19	0.19	1.57	0.17

Table 4-6. Weighted mean peak intensity ratio of each element to silicon in flyash B as compared to the corresponding overall ratio.

Element	Mean ratios of each element to silicon in each of the following size ranges given in μm . Shown also are the percentages of particles in each size range.					Weighted mean ratio	Overall ratio
	1 - 5 32.0	5 - 10 14.0	10 - 15 9.5	15 - 20 9.5	> 20 35.0		
Na	0.04	0.03	0.04	0.03	0.03	0.03	0.05
Mg	1.28	0.05	0.05	0.00	0.00	0.42	0.04
Al	0.63	0.40	0.45	0.40	0.63	0.56	0.29
K	0.18	0.24	0.07	0.06	0.05	0.12	0.01
Ca	10.50	2.25	0.37	0.58	0.64	3.99	1.73
Ti	0.69	0.34	0.08	0.17	0.14	0.34	0.12
	0.87	0.53	0.11	0.23	0.17	0.44	0.16

Table 4-7. Weighted mean peak intensity ratio of each element to silicon in flyash D as compared to the corresponding overall ratio.

Element	Mean ratios of each element to silicon in each of the following size ranges given in μm . Shown also are the percentages of particles in each size range.					Weighted mean ratio	Overall ratio
	1 - 5 12.0	5 - 10 10.5	10 - 15 13.0	15 - 20 14.5	> 20 50.0		
Na	0.00	0.00	0.00	0.00	0.00	0.00	0.00
Mg	0.00	0.00	0.00	0.00	0.00	0.00	0.00
Al	0.47	0.56	0.55	0.51	0.58	0.55	0.21
K	0.23	0.18	0.17	0.17	0.26	0.22	0.04
Ca	0.16	0.06	0.06	0.05	0.00	0.04	0.02
Ti	0.22	0.16	0.17	0.13	0.12	0.14	0.05
Fe	0.59	0.75	0.17	0.13	0.22	0.30	0.05

value times the percentage of particles in each size range can be calculated, and this summation is provided in the table as a "weighted mean ratio".

While the two sets of numbers represent very different things, these "weighted mean ratios" can be compared with the overall atomic ratios of the elements as calculated from the chemical analyses of Table 2-3. The latter are true chemical composition estimates; in contrast the former are merely peak intensity ratios, and are not direct estimates of composition without correction for various effects. The overall atom ratios are provided in the last column of each of the tables.

With a few specific exceptions, the numbers in the weighted mean ratio columns approximate the overall atom ratios within a factor of three. The exceptions are as follows:

- a) In all flyashes, the weighted mean ratio for K is much higher than its overall atom ratio (although all are small numbers).
- b) In flyashes A and D a similar gross disparity is found for Fe.
- c) In flyash B only a similar disparity is found for Mg.

Given the limitations of this study the results of these uncorrected EDXA determinations are considered to be congruent with the overall chemical compositions of the flyashes examined.

The following SEM micrographs are some examples of the kinds of particles that were sampled for the EDXA work. Figures 4-7 and 4-8 show two of the flyash A particles on which spot analyses were done. Figure 4-7 also shows the contrast between this particle with a diameter of about 50 μm and the finer particles.

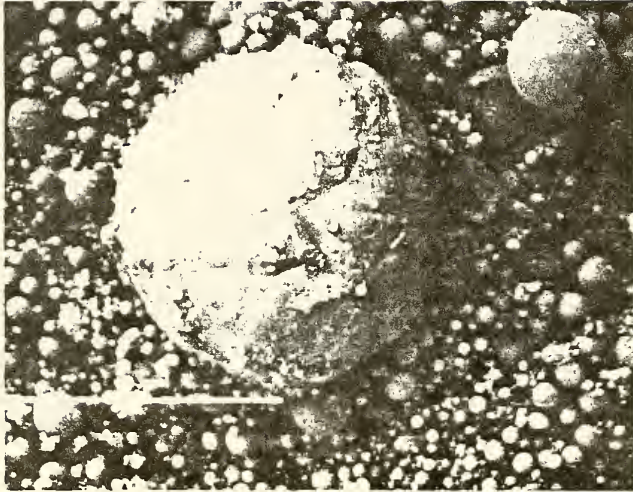


Fig. 4-7. Micrograph of flyash A particle at 1000 X magnification.

Figure 4-8 shows a particle with a diameter of about $17\ \mu\text{m}$. This seems to be an example of a hollow sphere which could be a plerosphere. In this case the spot analysis avoided the hole in the center of the particle.

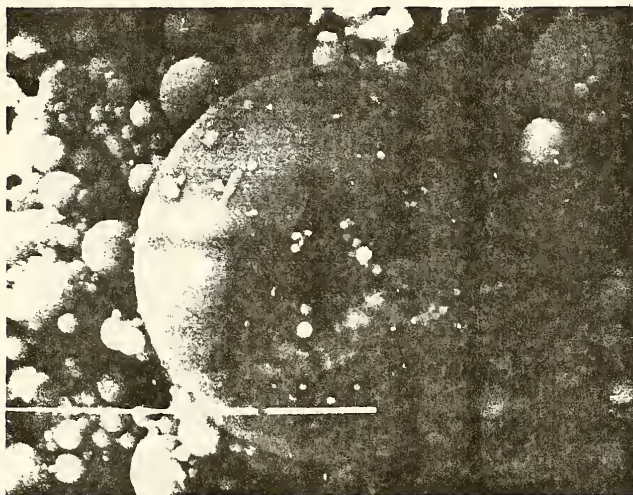


Fig. 4-8. Micrograph of flyash A particle at 3000 X magnification.

Figure 4-9 shows an irregularly shaped, hollow particle packed with spheres, thus being a plerosphere. This particle has a length of approximately $50\ \mu\text{m}$. The spot analyses were done following the scheme previously described, but avoiding holes and small particles on the surface.

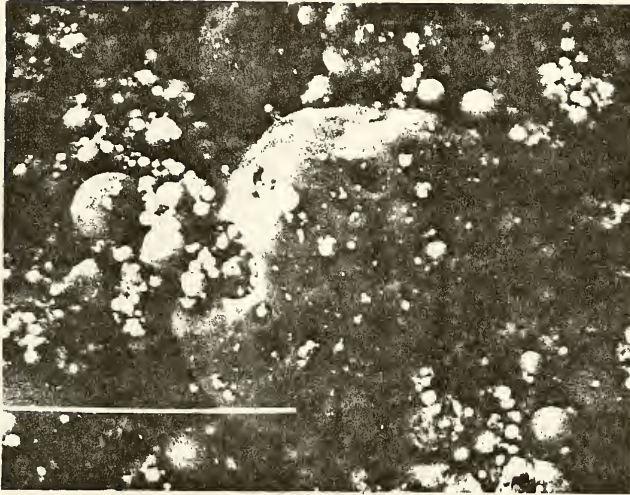


Fig. 4-9. Micrograph of flyash B particle at 1000 X magnification.

Figures 4-10 thru 4-12 show different flyash D particles. Figure 4-10 shows a plerosphere with a diameter of almost 40 μm . Figure 4-11 is a higher magnification micrograph. The center particle, used for spot analysis, has a diameter of about 5 μm . Figure 4-12 shows two "fused" particles which were not analyzed because they are not representative particles of the material.

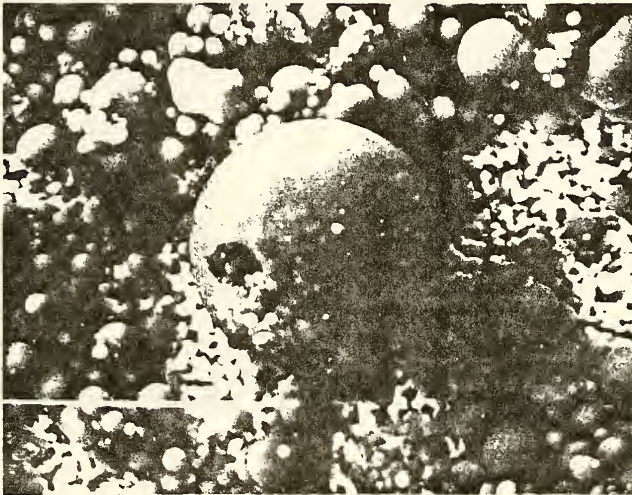


Fig. 4-10. Micrograph of a flyash D plerosphere at 1000 X magnification.

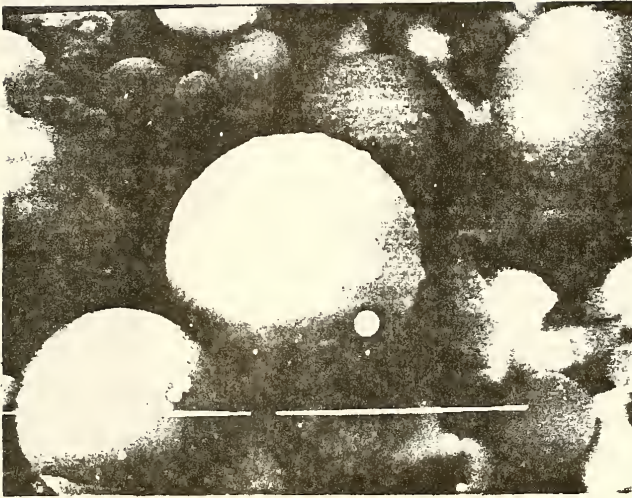


Fig. 4-11. Micrograph of flyash D particle at 7000 X magnification.

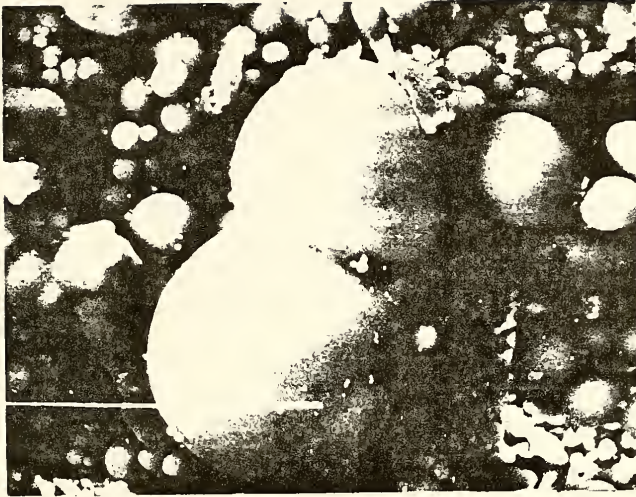


Fig. 4-12. Micrograph of "fused" flyash D particles at 1500 X magnification.

Setting Time

Table 4-8 shows the setting times for the pastes under study as well as for the reference portland cement paste.

Table 4-8. Setting times for cement-flyash pastes.

System	Initial set,		Final set,	
	h	min	h	min
Reference cement	3	00	4	20
A	7	10	11	15
B	5	10	11	04
C	5	05	9	15
D	5	15	11	00
E	5	00	12	20

With respect to the reference cement paste, as a standard basis, the following observations were made. Pastes containing flyashes B, C, D, and E had their initial set retarded by approximately two hours, which is a 70 percent increase in time. Paste with flyash A suffered a 140 percent increase in its time of initial set, showing a four-hour retardation. The final set

occurred in these flyash pastes, on an average, seven hours later than in the reference cement. However, it must be pointed out that flyash C had the earliest final setting - approximately five hours later than the reference cement. The times of final set are between 200 and 300 percent higher than for the reference paste.

Temperature Evolution

The evolution of temperature during hydration was followed for each of the cement-flyash pastes. Figure 4-13 shows the temperature increase curves for the cement-flyash pastes as well as the curve for the reference portland cement paste. Temperature evolution in each case was recorded as a continuous function; however to avoid confusion due to extensive overlapping, the plots in Figures 4-13 and 4-14 are shown discontinuously as discrete points. Figure 4-14 shows the first four hours of these curves.

All these are single-peak curves and, with the exception of the curve for system A, they all show a dormant period of about three hours, after which time a sharp increase in temperature is observed. In the case of system A the dormant period lasts about five hours.

As expected the reference portland cement paste reached the highest temperature, with its maximum appearing 280 min after its final set. The curves for systems B and C are similar in their temperature evolution. However, the curve for system C paste shows a maximum more than two hours after its final set and the curve for system B paste shows a maximum an hour before its final set. For the first couple of hours the paste with flyash B maintains the highest level of temperature, even higher than that of the reference cement. This suggests a vigorous pre-dormant period.

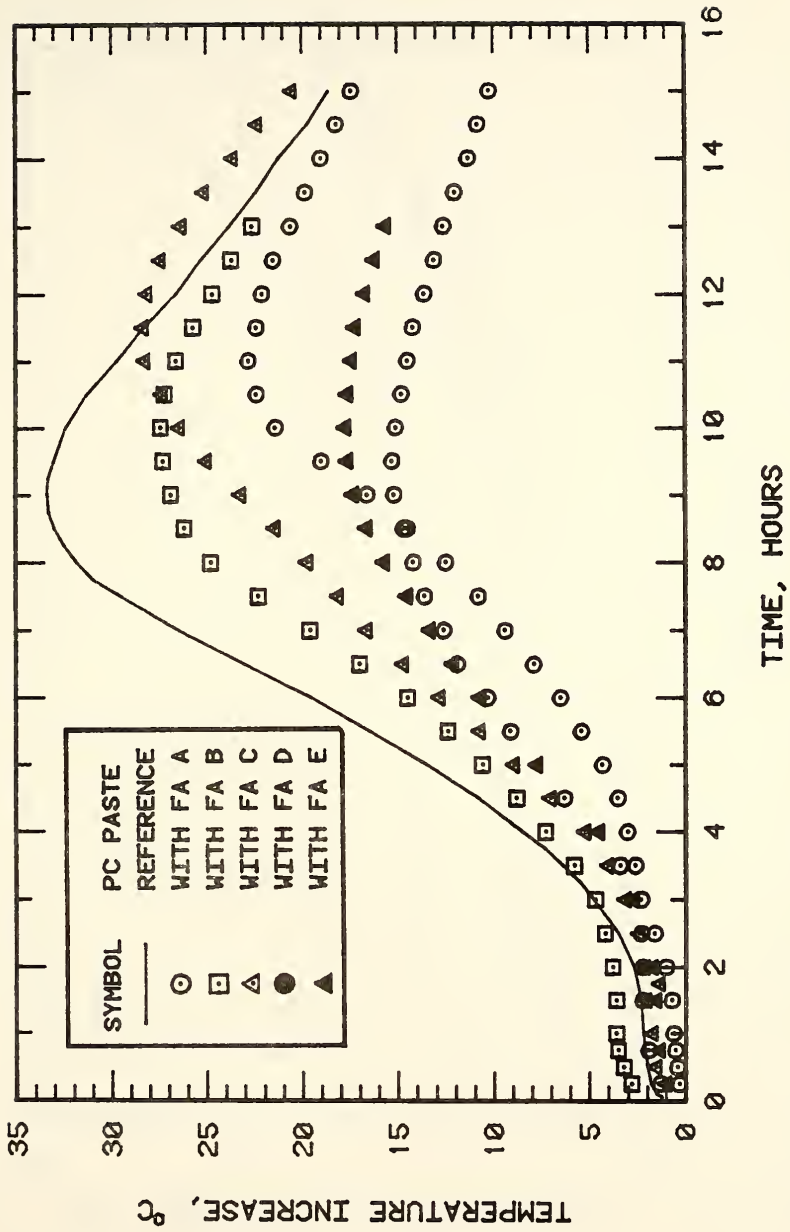


Fig. 4-13. Temperature increase in cement-flyash pastes and reference cement paste.

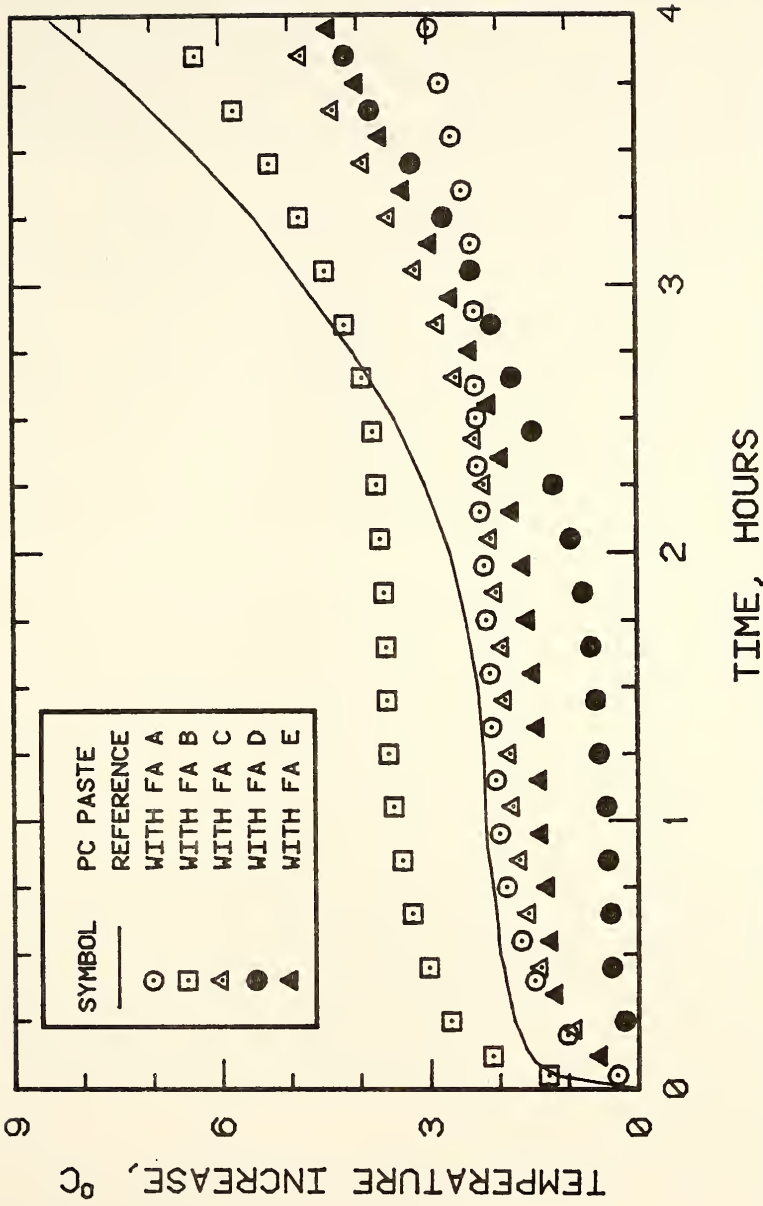


Fig. 4-14. Temperature increase in cement-flyash pastes and reference cement paste during the first four hours of hydration.

In Figure 4-14 it can be seen that systems D and E have similar curves showing the lowest temperature maxima of the systems studied. The curve for system D reaches its maximum about 1 1/2 hours before its final set. The curve for system E shows a maximum more than 2 hours before final set.

Table 4-9 shows the temperatures and times for the maxima of the temperature evolution curves compared to the corresponding times of set.

From a comparison of the temperature evolution curves it can be seen that flyashes B and C seem to be more reactive than the other flyashes studied; the maximum temperature evolved in cement-flyash pastes prepared with these flyashes is close to that of the reference cement paste. Following the same reasoning, flyashes D and E seem to be more inert than the others.

Non-Evaporable Water Determinations

The percentage of non-evaporable water was determined on all cement-flyash pastes from which pore solution was expressed. The results given in Table 4-10 are values corrected for loss on ignition of cement and flyash. These data give an idea of the degree of hydration. It is interesting to note the similarities between system A and the reference cement. At 180 days these two systems have reached a rather high degree of hydration. The other four systems all show very similar values at 180 days, values which are slightly lower than those observed in the reference cement and in system A.

Table 4-9. Temperature evolution maxima compared to time of set in cement-flyash pastes.

<u>System</u>	<u>Temperature evolution maximum temp., °C</u>	<u>Temperature evolution maximum time, min</u>	<u>Initial set time, min</u>	<u>Final set time, min</u>
Reference cement	33.5	540	180	260
A	22.7	660	430	675
B	27.4	600	310	664
C	28.3	690	305	555
D	15.2	570	315	660
E	17.6	600	300	740

Table 4-10. Non-evaporable water content in cement-flyash pastes at different ages, percent.

Age, hours	Reference cement	Systems				
		A	B	C	D	E
1	8.4	7.2	6.5	8.0	3.1	4.2
2	8.7	8.8	---	---	---	---
3	---	---	5.7	7.9	3.4	5.7
4	8.4	6.6	---	---	---	---
6	7.4	6.0	6.0	8.3	3.5	4.3
10	7.6	6.5	5.7	7.4	4.6	5.6
14	9.0	7.9	6.8	8.1	5.2	6.6
18	9.1	8.7	7.3	9.1	5.6	7.6
24	9.9	9.4	8.1	8.6	6.0	7.4
72	10.6	10.5	10.6	11.1	10.6	10.8
168	12.7	11.8	9.7	9.5	8.2	8.8
672	13.1	12.1	11.4	11.0	11.2	10.8
2160	15.4	15.6	14.5	13.4	12.5	13.0
4320	17.0	16.8	15.4	14.8	14.2	14.2

Chemical Analyses of Pore Solutions

Pore solutions of pastes from all five cement-flyash systems and from the reference cement were analyzed for Ca^{2+} , K^+ , Na^+ , SO_4^{2-} , and OH^- at the following ages: 1, 3, 6, 10, 14, 18, and 24 hours, and also at 3, 7, 28, 90, and 180 days. Analyses for 2 and 4 hours were obtained for the reference cement and for system A instead of the 3 hour analyses.

Table 4-11 gives the pore solution concentration of the ions found. These values have been adjusted to the basis of the initial water content using a concentration correction factor calculated from the values of non-evaporable water content of Table 4-10. Appendix C shows the concentrations of the ionic species in the pore solutions with no adjustment for change in water content. The last column of Table 4-11 shows the charge balance of the ionic species in the pore solution at each age. These results are reasonable and within the experimental error expected of such determinations.

The adjusted ionic concentrations determined as a function of time of hydration for each system are plotted in Figures 4-15 thru 4-20. A logarithmic scale was chosen to show these concentrations, as normalities, to allow a better observation of the behavior of calcium in the pore solutions. The time scale is also given on a logarithmic scale to permit presentation of all results on one graph for each system. The use of a full logarithmic plot does not give a good picture of the proportionate increase of OH^- with the decrease of SO_4^{2-} . However, a close look will reveal a good relationship between these two curves for all systems studied.

Table 4-11. Measured normality of ionic species in paste pore solutions as a function of time (adjusted for change in water content).

Age, hours	Ca ²⁺	K ⁺	Na ⁺	SO ₄ ²⁻	OH ⁻	Charge balance
Reference Portland Cement Paste						
1	0.0387	0.2421	0.0265	0.1426	0.1335	+0.0312
2	0.0368	0.2404	0.0269	0.1389	0.1311	+0.0341
4	0.0359	0.2442	0.0280	0.1536	0.1287	+0.0258
6	0.0350	0.2534	0.0295	0.1721	0.1262	+0.0196
10	0.0332	0.2542	0.0300	0.1712	0.1205	+0.0257
14	0.0098	0.2559	0.0305	0.0686	0.2059	+0.0217
18	0.0062	0.2591	0.0304	0.0347	0.2523	+0.0087
24	0.0051	0.2599	0.0302	0.0202	0.2732	+0.0018
72	0.0051	0.2577	0.0347	0	0.3053	-0.0078
168	0.0043	0.2577	0.0348	0	0.3123	-0.0155
672	0.0019	0.2751	0.0452	0	0.3216	+0.0006
2160	0	0.2624	0.0425	0	0.2856	+0.0193
4320	0	0.2435	0.0357	0	0.2599	+0.0193
Paste with Flyash A						
1	0.0363	0.1753	0.0263	0.1176	0.1047	+0.0156
2	0.0383	0.1707	0.0264	0.1063	0.1114	+0.0177
4	0.0373	0.1779	0.0287	0.1316	0.1218	-0.0095
6	0.0370	0.1803	0.0292	0.1488	0.1228	-0.0251
10	0.0379	0.1849	0.0302	0.1204	0.1166	+0.0160
14	0.0089	0.1944	0.0333	0.0163	0.2140	+0.0063
18	0.0069	0.1999	0.0363	0	0.2354	+0.0077
24	0.0063	0.1964	0.0368	0	0.2335	+0.0060
72	0.0043	0.2205	0.0632	0	0.2920	-0.0040
168	0.0043	0.2226	0.0753	0	0.3198	-0.0176
672	0.0019	0.2289	0.1042	0	0.3379	-0.0029
2160	0	0.2005	0.1131	0	0.2947	+0.0189
4320	0	0.1896	0.0990	0	0.2770	+0.0116

Table 4-11, continued.

<u>Age, hours</u>	<u>Ca²⁺</u>	<u>K⁺</u>	<u>Na⁺</u>	<u>SO₄²⁻</u>	<u>OH⁻</u>	<u>Charge balance</u>
Paste with Flyash B						
1	0.0361	0.1688	0.2497	0.2905	0.1414	+0.0227
3	0.0369	0.1719	0.2542	0.2900	0.1548	+0.0182
6	0.0246	0.1834	0.2618	0.2738	0.1728	+0.0232
10	0.0052	0.1894	0.2712	0.0326	0.4081	+0.0251
14	0.0034	0.1933	0.2698	0	0.4597	+0.0068
18	0.0037	0.1941	0.2703	0	0.4669	+0.0012
24	0.0031	0.1926	0.2669	0	0.4557	+0.0069
72	0.0035	0.2023	0.2646	0	0.4794	-0.0090
168	0.0030	0.2171	0.2887	0	0.5296	-0.0208
672	0.0018	0.2115	0.3271	0	0.5270	+0.0134
2160	0	0.1894	0.3026	0	0.4297	+0.0623
4320	0	0.1827	0.2783	0	0.4070	+0.0540
Paste with Flyash C						
1	0.0378	0.1772	0.3395	0.3527	0.1549	+0.0469
3	0.0371	0.1780	0.3404	0.3494	0.1610	+0.0451
6	0.0335	0.1787	0.3373	0.3605	0.1453	+0.0437
10	0.0128	0.1952	0.3628	0.2867	0.2409	+0.0432
14	0.0057	0.1907	0.3458	0.1230	0.3560	+0.0632
18	0.0030	0.1934	0.3375	0.0366	0.4928	+0.0045
24	0.0024	0.2061	0.3557	0.0123	0.5494	+0.0025
72	0.0027	0.2099	0.3676	0	0.5795	+0.0007
168	0.0027	0.2227	0.4236	0	0.6577	-0.0087
672	0.0017	0.2437	0.5126	0	0.7448	+0.0132
2160	0	0.2430	0.5828	0	0.7465	+0.0793
4320	0	0.2345	0.4840	0	0.6820	+0.0365

Table 4-11, continued.

<u>Age, hours</u>	<u>Ca²⁺</u>	<u>K⁺</u>	<u>Na⁺</u>	<u>SO₄²⁻</u>	<u>OH⁻</u>	<u>Charge balance</u>
Paste with Flyash D						
1	0.0454	0.1780	0.0211	0.1063	0.1242	+0.0140
3	0.0435	0.1782	0.0208	0.1077	0.1197	+0.0151
6	0.0405	0.1763	0.0227	0.1197	0.1150	+0.0048
10	0.0180	0.1769	0.0227	0.0552	0.1406	+0.0218
14	0.0104	0.1837	0.0231	0.0392	0.1896	-0.0116
18	0.0075	0.1867	0.0232	0.0179	0.2132	-0.0137
24	0.0067	0.1929	0.0240	0.0203	0.2276	-0.0243
72	0.0040	0.1949	0.0304	0	0.2263	+0.0030
168	0.0046	0.2072	0.0310	0	0.2521	-0.0093
672	0.0030	0.1861	0.0313	0	0.2141	+0.0063
2160	0	0.1629	0.0387	0	0.1971	+0.0045
4320	0	0.1527	0.0399	0	0.1675	+0.0251
Paste with Flyash E						
1	0.0490	0.1766	0.0217	0.1025	0.1306	+0.0142
3	0.0427	0.1715	0.0212	0.1003	0.1194	+0.0157
6	0.0405	0.1793	0.0226	0.1158	0.1125	+0.0141
10	0.0252	0.1794	0.0225	0.0849	0.1314	+0.0108
14	0.0139	0.1770	0.0230	0.0517	0.1628	-0.0006
18	0.0090	0.1759	0.0226	---	0.1838	+0.0237
24	0.0062	0.1824	0.0234	0.0138	0.2131	-0.0149
72	0.0046	0.1940	0.0278	0	0.2291	-0.0027
168	0.0052	0.2122	0.0320	0	0.2592	-0.0098
672	0.0040	0.2116	0.0362	0	0.2457	+0.0061
2160	0	0.2001	0.0372	0	0.2339	+0.0034
4320	0	0.1920	0.0298	0	0.2017	+0.0201

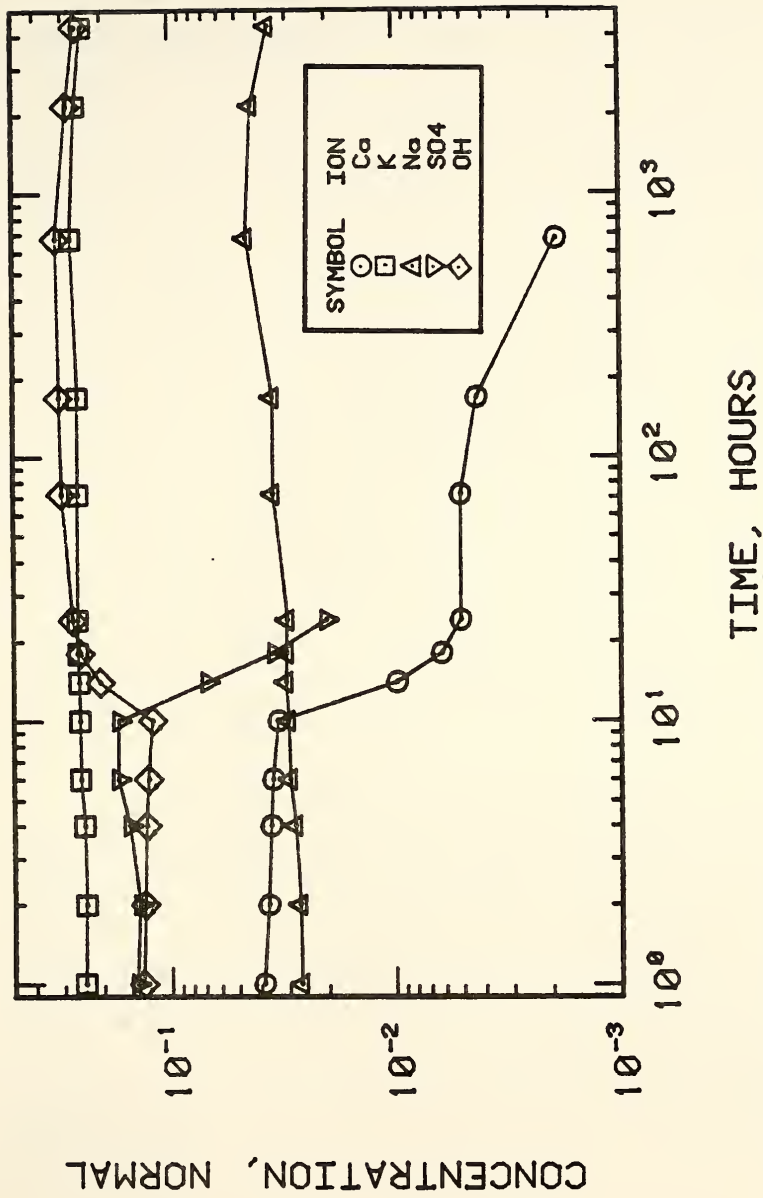


Fig. 4-15. Concentration of ions in reference cement paste pore solution as a function of time.

In the reference cement pore solution there is a clear and distinct point after which there is a steep fall out of solution of SO_4^{2-} and Ca^{2+} . At this point, which appears at 10 hours, there is also a sharp increase in the concentration of OH^- . Presumably the formation of ettringite and the precipitation of calcium hydroxide are responsible for the removal of SO_4^{2-} and Ca^{2+} from the pore solution. The concentration of OH^- in the pore solution increases with time. Since the previous reactions do not involve all of the OH^- present, then this anionic species must be related to another reaction. This must be a hydrolysis reaction other than the dissolution of gypsum, which is soon depleted. A hydrolysis of calcium silicates on the surface grains of cement is suspected to be responsible for the increasing concentrations of OH^- in the pore solutions. The cations, Na^+ and K^+ , show only slight increases in concentration as a function of time.

The patterns followed by the concentrations of ions in the pore solution of pastes containing flyash A are in agreement with those of the reference cement regarding the time of the sudden change of concentrations. Here again, the decrease of SO_4^{2-} and Ca^{2+} occurs at 10 hours with a concomitant increase in OH^- .

Figure 4-16 shows the ion concentrations in pore solutions expressed at different ages from system A pastes. Overall the curves for each ionic species are very similar to those of the reference cement paste. However two differences are notable. The latest age at which the SO_4^{2-} ion is found in the pore solution of system A pastes is at 14 hours as compared with a 24 hour presence in the reference cement paste. The concentration of Na^+ in the pore solution of system A pastes shows a fourfold increase as compared with the less than twofold increase in the reference cement pastes.

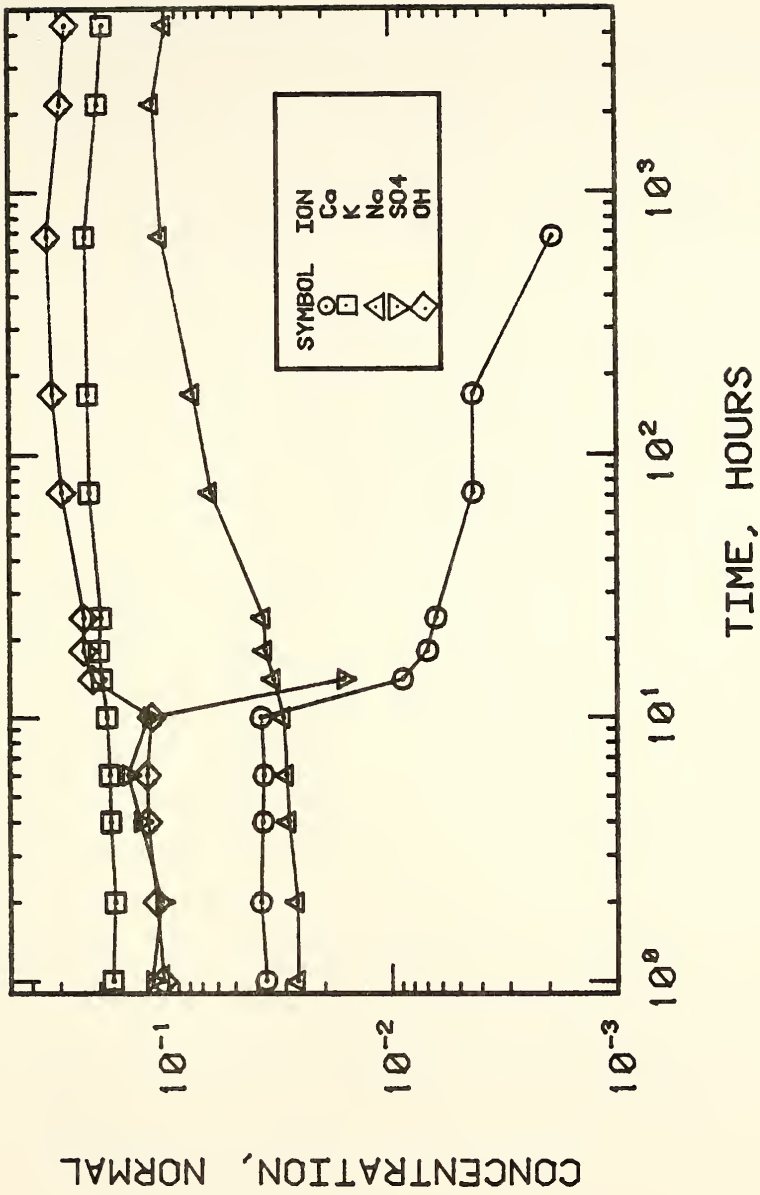


Fig. 4-16. Concentration of ions in system A paste pore solution as a function of time.

Pastes containing flyashes B and C are very different from both the reference cement paste and pastes containing flyash A with respect to their pore solutions. Figures 4-17 and 4-18 show the ion concentrations in the pore solutions of these systems. Even though flyashes A, B, and C are all ASTM class C flyashes, the chemical composition of the last two strongly affects their pore solution composition.

The SO_3 contents of flyashes B and C are higher than that of flyash A and this is reflected in the higher levels of sulfate in their pore solutions. At early ages the sulfate concentrations of these two systems is twice as high as that of the reference portland cement paste. In system B there is an abrupt fall after 10 hours and it is no longer detected. In system C pastes the SO_4^{2-} concentration, at 18 hours, is equivalent to that of the reference cement paste, and it is still found at 24 hours.

The Na_2O content of flyashes B and C is higher than that of flyash A. This gives rise to a ten times higher concentration of Na^+ in the pore solution of the paste containing flyash B than that determined in the reference cement paste. The paste with flyash C shows an even higher concentration of Na^+ in its pore solution.

The high levels of OH^- reached in the pore solutions of the pastes with flyashes B and C are distinct features of these two systems. Almost twice as high a concentration of OH^- is found in the pore solution of flyash B pastes as that in the reference cement paste. In the pore solution of flyash C paste the concentration of OH^- starts a little higher than that in the portland cement reference paste; it steadily increases until at later ages it is higher than twice the corresponding concentration in the reference cement paste.

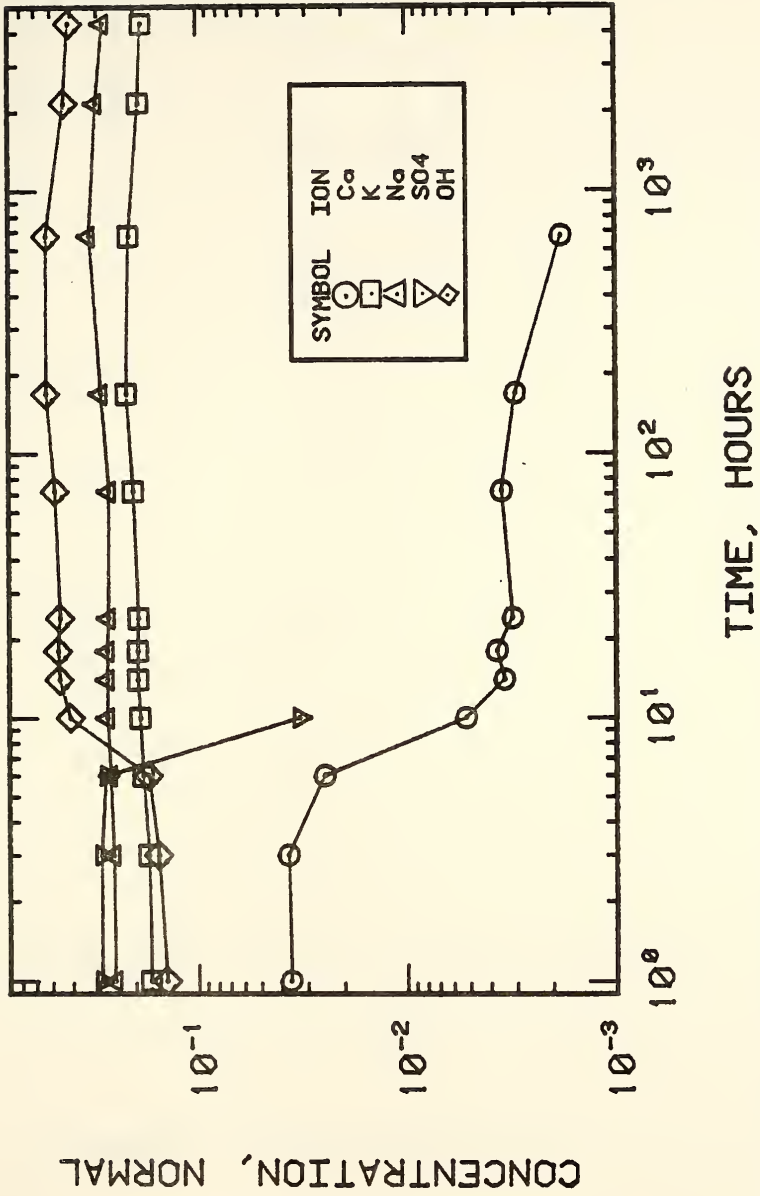


Fig. 4-17. Concentration of ions in system B pore solution as a function of time.

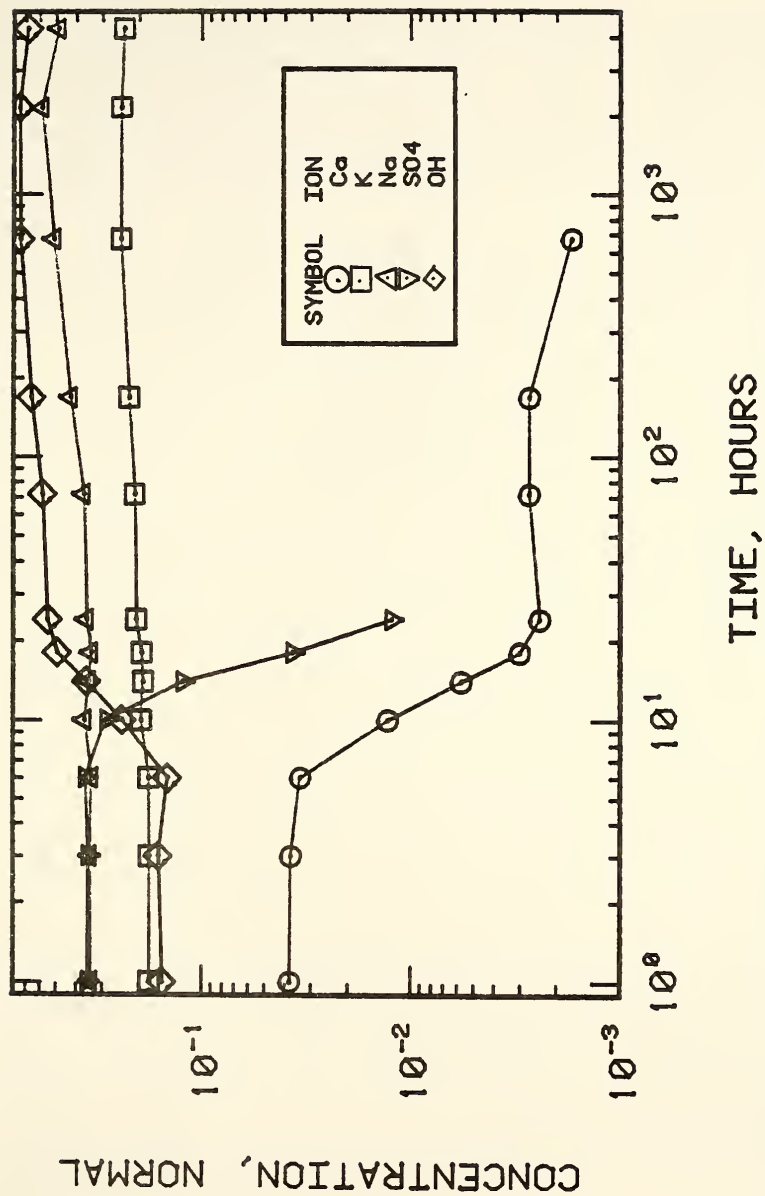


Fig. 4-18. Concentration of ions in system C paste pore solution as a function of time.

The effect of K_2O from the flyashes is negligible in the pore solutions of the flyash B and C cement pastes. Calcium concentrations are equivalent to those of the portland cement reference paste at early ages and then fall off to give the expected proportional concentrations of a 30 percent substitution of cement by flyash.

The pastes with flyashes D and E both contain class F flyashes. In these two systems the pore solution concentrations are, with the exception of calcium, lower than the concentrations in the reference pastes by approximately 30 percent. This indicates the inert character of these flyashes. Figures 4-19 and 4-20 show the curves for the ion concentrations in pore solutions of cement pastes bearing flyashes D and E through time.

The measured concentrations of calcium in the pore solutions of these systems are slightly higher than that of the reference cement paste, but it is not certain whether the differences are significant or not. The patterns of the other ions are very similar to the patterns for the corresponding ions in the reference paste, with the exception that they are generally about 30 percent lower on the concentration scale. In the flyash D and flyash E systems, sulfate is still detected at 24 hours.

As mentioned at the beginning of this section, there is a point in the time scale where dramatic changes in the levels of SO_4^{2-} , Ca^{2+} , and OH^- occur. For the reference cement paste and for the paste with flyash A this happens at 10 hours. In the plots for the pastes with flyashes B, C, D, and E it is seen that this point appears at about 6 hours. There is no obvious relation between this behavior in the pore solutions and other observed characteristics of the corresponding pastes such as setting time and time of maximum temperature evolution. However, coincidentally the highest temperature evolution is observed in the flyash-bearing cement pastes with the highest OH^- concentrations, that is, systems B and C.

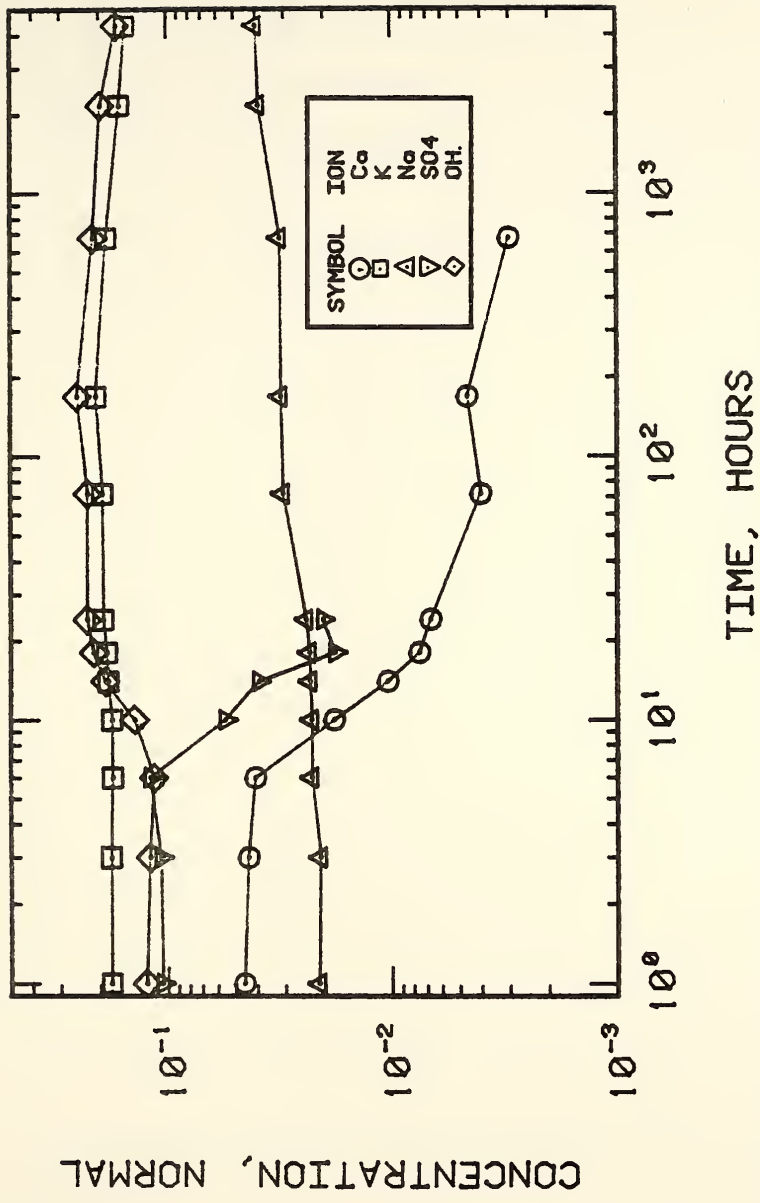


Fig. 4-19. Concentration of ions in system D paste pore solution as a function of time.

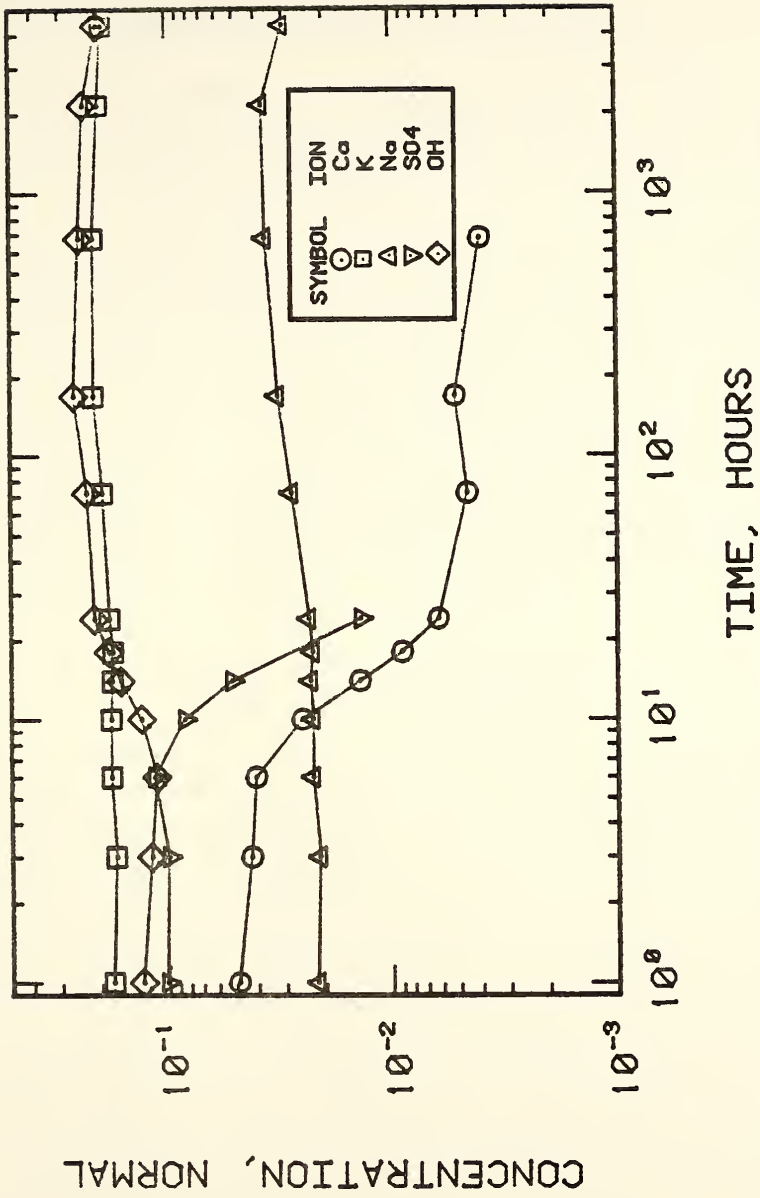


Fig. 4-20. Concentration of ions in system E paste pore solution as a function of time.

Compressive Strength of Mortar Cubes

The compressive strength of mortar cubes as a function of time is shown in Table 4-12. The values in the table represent the means of four tested cubes; also given are the standard deviations.

Figures 4-21 and 4-22, which are plots of the compressive strengths of the mortar cubes on a logarithmic time scale, show the expected higher compressive strength for the portland cement reference mortar cubes during the first seven days. At 28 days, the mortar cubes bearing flyash A attained a higher strength than the reference mortar cubes. By 180 days all flyash bearing mortar cubes reached at least as high a strength as the reference mortar cubes, approximately 6000 psi. Thus the flyashes differ in their effects on early strength, but differ comparatively little in their effects on later strength.

Length Changes in Mortar Bars

Four mortar bars were prepared for each cement-flyash system and for the portland cement reference system. The bars were measured 24 hours after molding. This reading was used as the initial reference length in all calculations. All subsequent readings of the bars were corrected relative to the variations of the comparator bar. All readings were taken in the constant temperature, constant humidity room.

The results of length-change measurements, reported as percent strain, are shown in Appendix D, and are presented in graphical form in Figures 4-23 thru 4-28. It can be seen that the mortar bars prepared with flyash C are the only ones that show a significant expansion due to the alkali-silica reaction. These results are presumably associated with the chemical composition of flyash C.

Table 4-12. Compressive strength of mortar cubes prepared with different flyashes, Psi, and corresponding standard deviations shown in parentheses.

Age, days	Reference mortar	Systems				
		A	B	C	D	E
1	1400	710	1130	1030	940	670
	(103)	(110)	(110)	(20)	(110)	(40)
3	3020	2370	2470	2720	1790	1720
	(250)	(150)	(230)	(200)	(140)	(130)
7	3580	3290	3530	3340	2580	2570
	(560)	(400)	(260)	(150)	(180)	(210)
28	5020	5570	4660	4680	4050	4270
	(420)	(190)	(190)	(270)	(160)	(110)
90	5630	6150	5480	5350	5410	5810
	(250)	(430)	(740)	(170)	(310)	(290)
180	5560	6910	6590	5700	5590	6180
	(150)	(330)	(210)	(660)	(720)	(390)

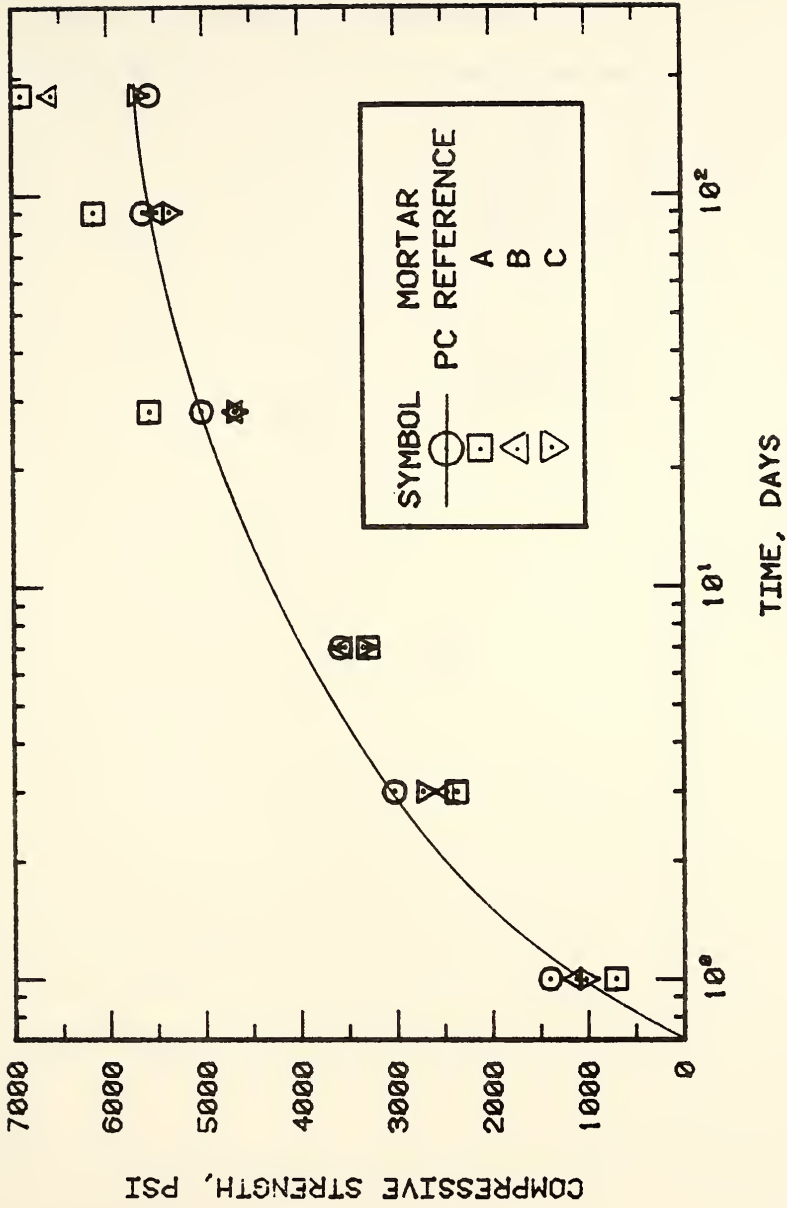


Fig. 4-21. Compressive strengths of mortar cubes bearing flyashes A, B, and C.

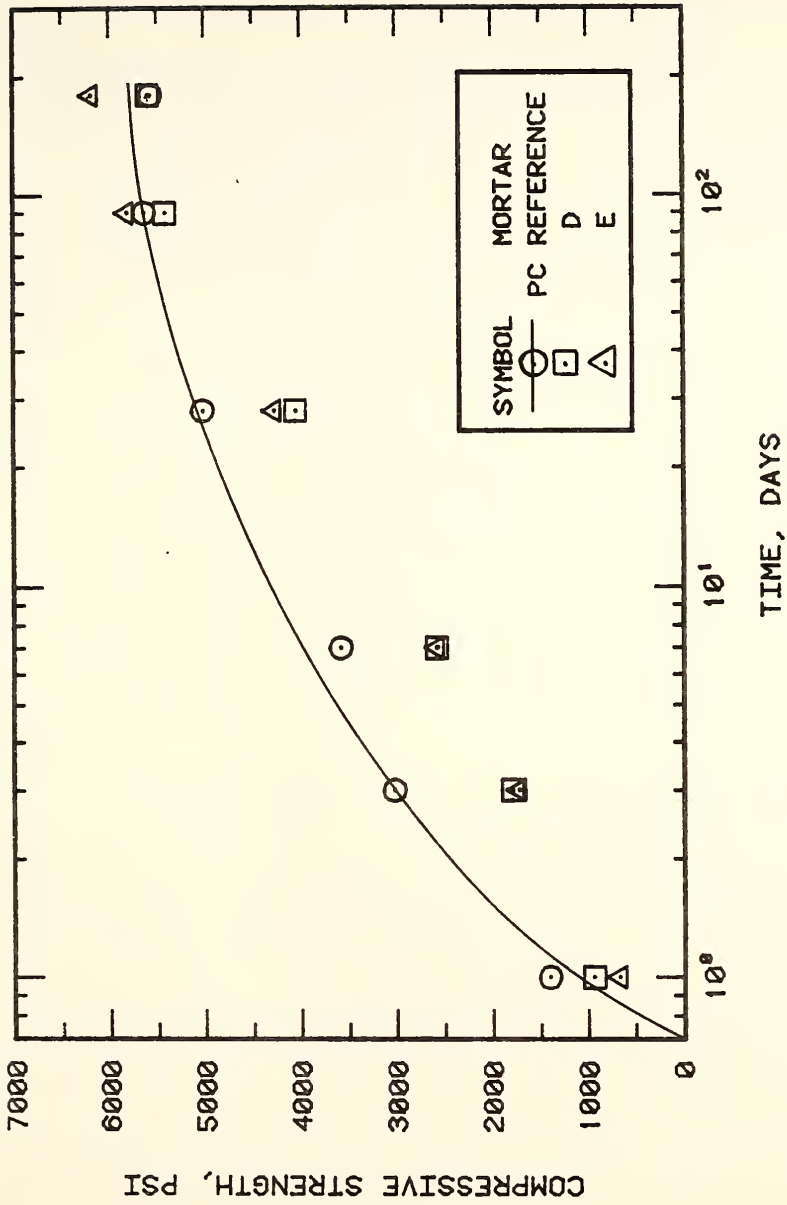


Fig. 4-22. Compressive strengths of mortar cubes bearing flyashes D and E.

From the chemical analyses of the flyashes (Table 2-3), it is observed that flyash C has the highest content of Na of all the flyash samples, expressed as 4.1 percent Na_2O . Looking at the pore solution analysis (Table 4-11), it can be seen that system C pastes have the highest concentration of Na^+ and OH^- of all the cement-flyash paste pore solutions, much higher than that of the reference paste pore solution. If the alkali-silica reaction is a through-solution reaction, then this is an explanation of the expansion observed in system C mortar bars.

Flyash B also has a relatively high content of Na_2O . As can be seen from Figure 4-25, mortar bars containing this flyash are the only other group of bars that show any increase in length. However, the expansion of system B mortar bars does not seem to be significant.

The other bars behave similarly to the reference mortar bars except that system E mortar bars show about twice as much shrinkage at 320 days as the reference mortar bars. During the course of the measurements the system E bars were consistently noted as appearing drier than the other bars, despite the identical conditions of storage.

Analytical determinations were made of the flyashes and of the cement used in these studies in order to determine the amounts of water-soluble alkalies in each of these components. The method used was that of Paragraph 17.2 of ASTM Designation C 114-81, which involves adding a tenfold amount of water to a weighted amount of the component, shaking for 10 minutes, filtering, and determining the sodium and potassium contents of the filtrate. The resulting data are shown in Table 4-13.

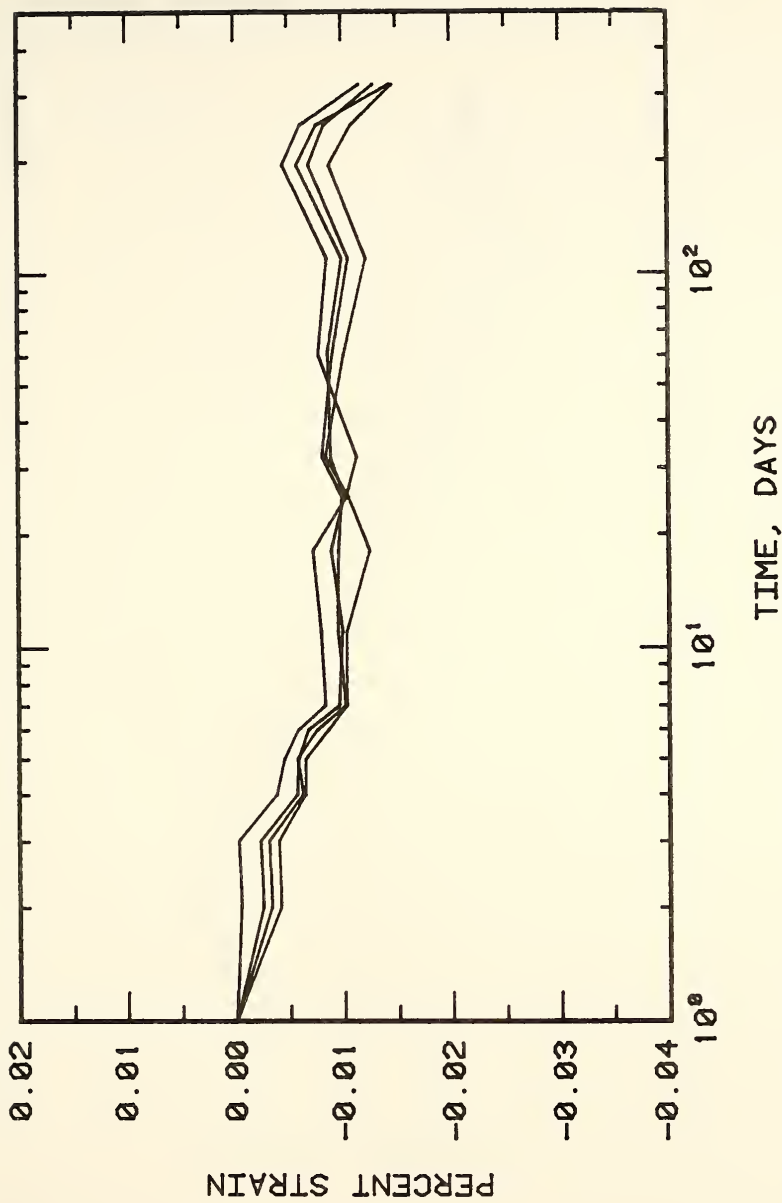


Fig. 4-23. Length change of reference cement mortar bars.

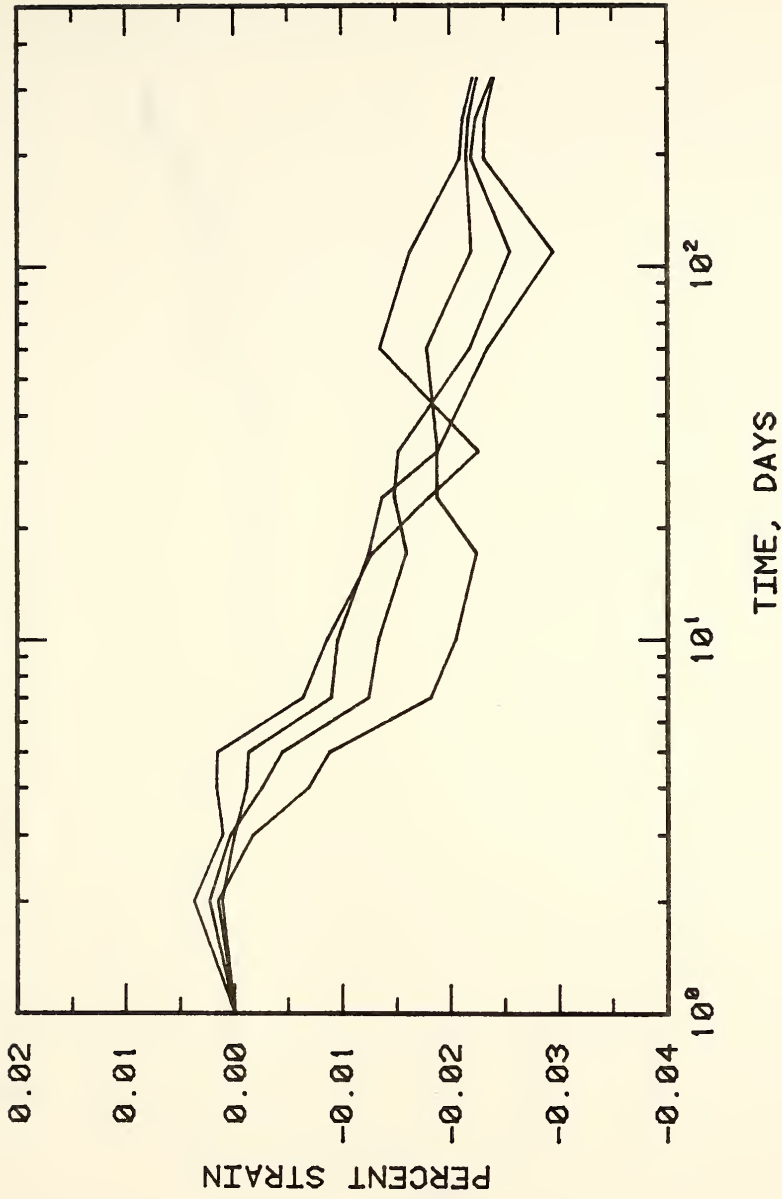


Fig. 4-24. Length change of system A mortar bars.

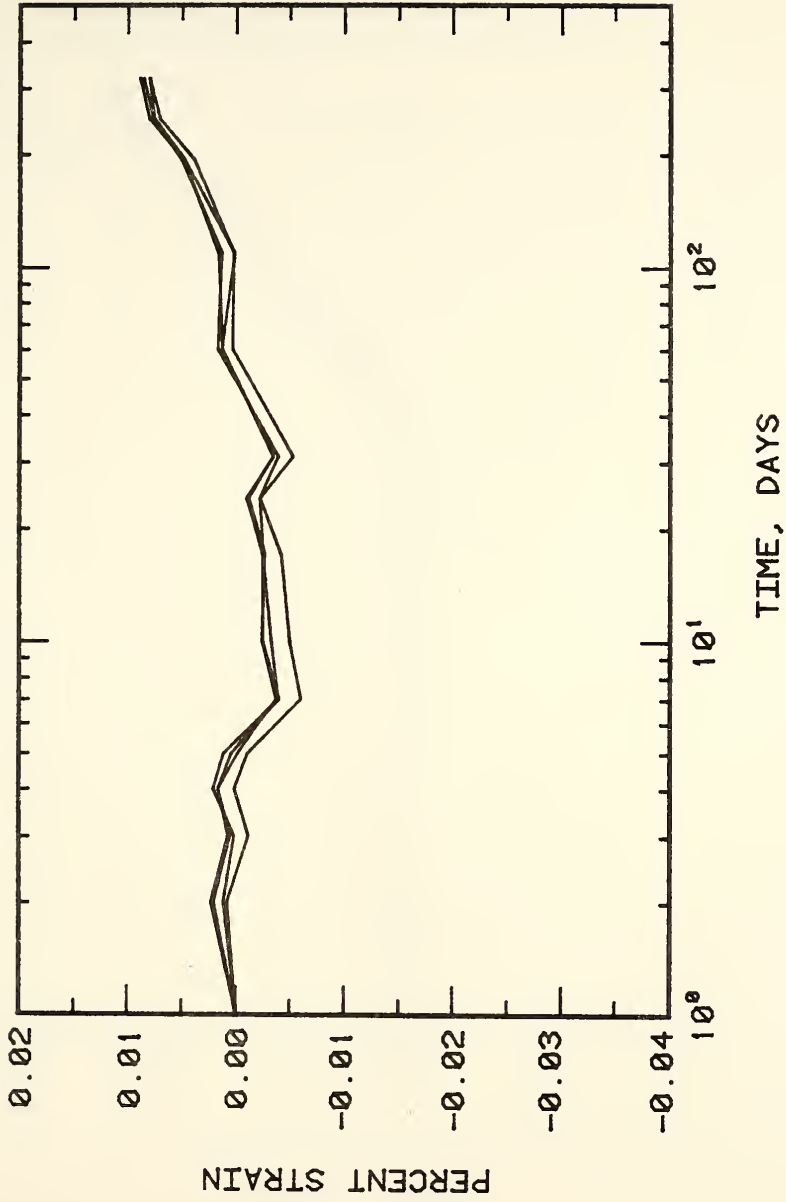


Fig. 4-25. Length change of system B mortar bars.

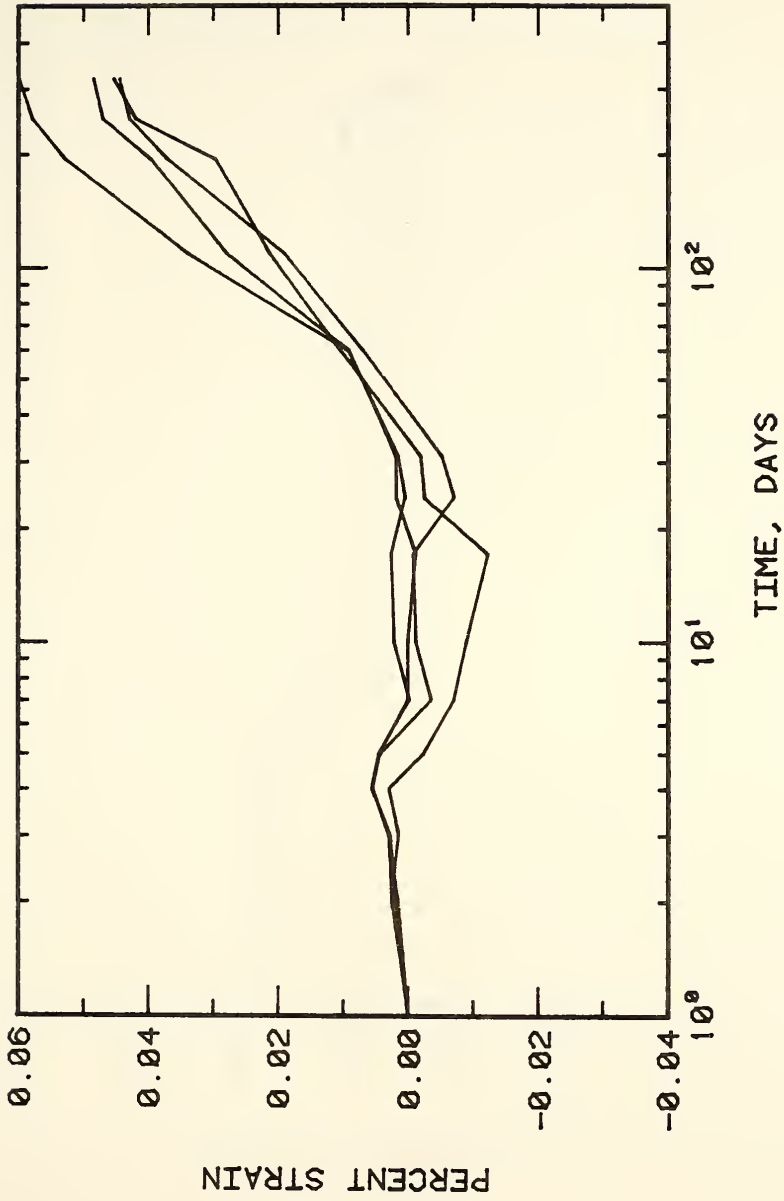


Fig. 4-26. Length change of system C mortar bars.

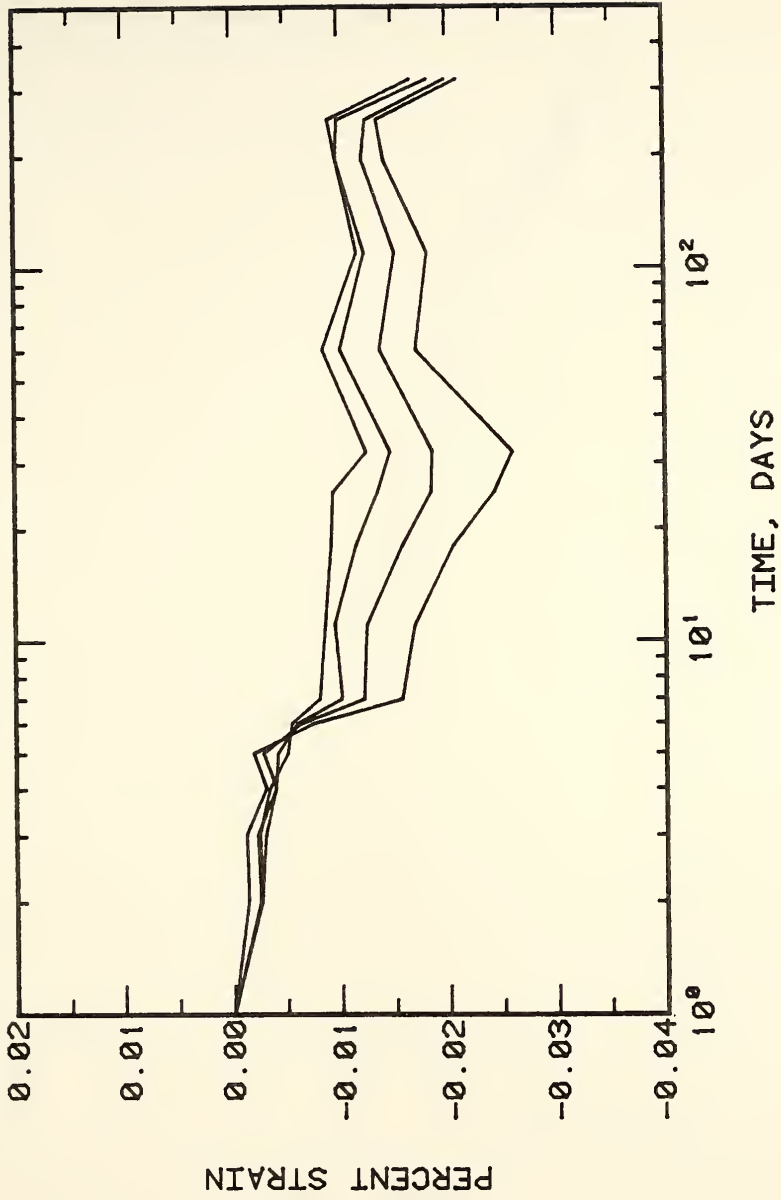


Fig. 4-27. Length change of system D mortar bars.

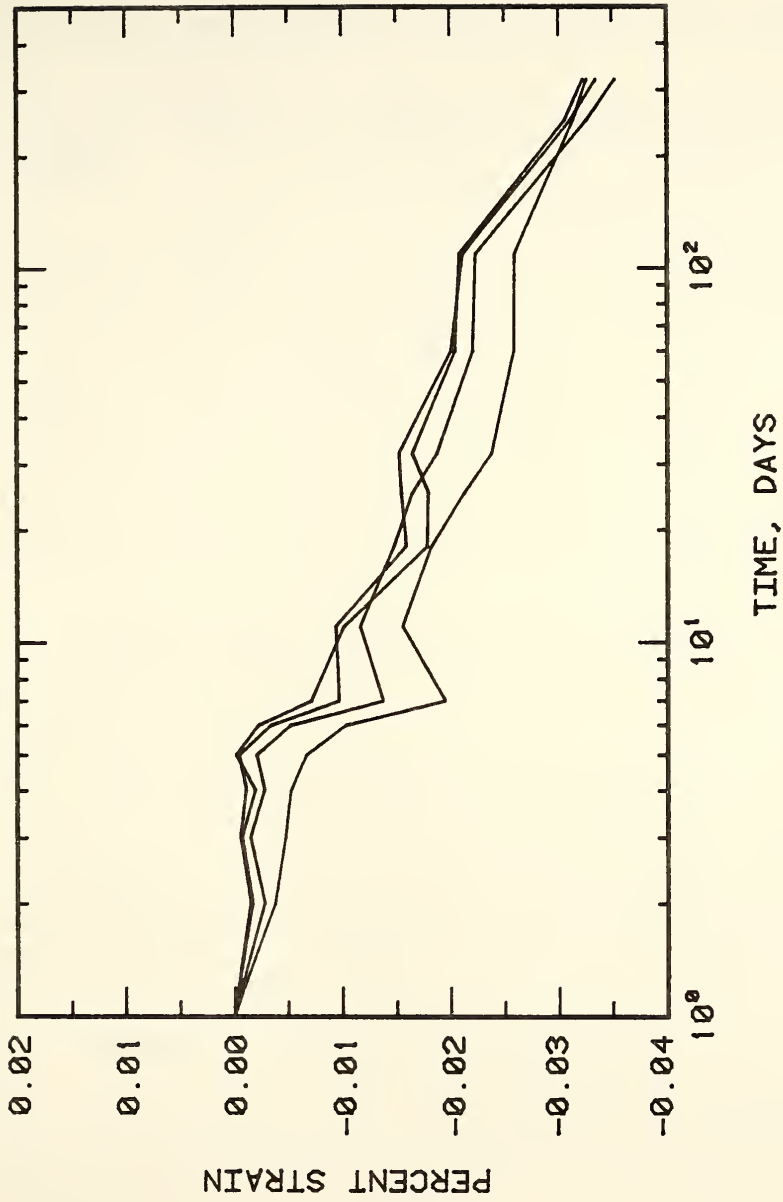


Fig. 4-28. Length change of system E mortar bars.

Table 4-13. Water-soluble alkalis in cement and flyashes used.

Material	Water soluble Na ₂ O, %	Water soluble K ₂ O, %	Total water soluble alkalies, as % Na ₂ O
Portland cement	0.08	0.54	0.45
Flyash A	0.38	0.12	0.45
Flyash B	1.25	0.17	1.36
Flyash C	2.20	0.34	2.42
Flyash D	0.20	0.48	0.33
Flyash E	0.04	0.73	0.51

The calculated percentages of water-soluble alkalis produced in the mixtures of 70 percent portland cement - 30 percent flyash used in these mortar bars were then respectively 0.45, 0.73, 1.04, 0.42, and 0.47 percent Na₂O equivalent for mixes made with flyashes A, B, C, D, and E respectively. Only the flyash C mix (1.04 percent Na₂O equivalent) showed significant expansion; the flyash B mix (0.73 percent Na₂O equivalent) showed borderline expansion, and the other three mixes (0.42 to 0.47 percent Na₂O equivalent) showed net shrinkage.

Compressive Strength of Concrete Cylinders

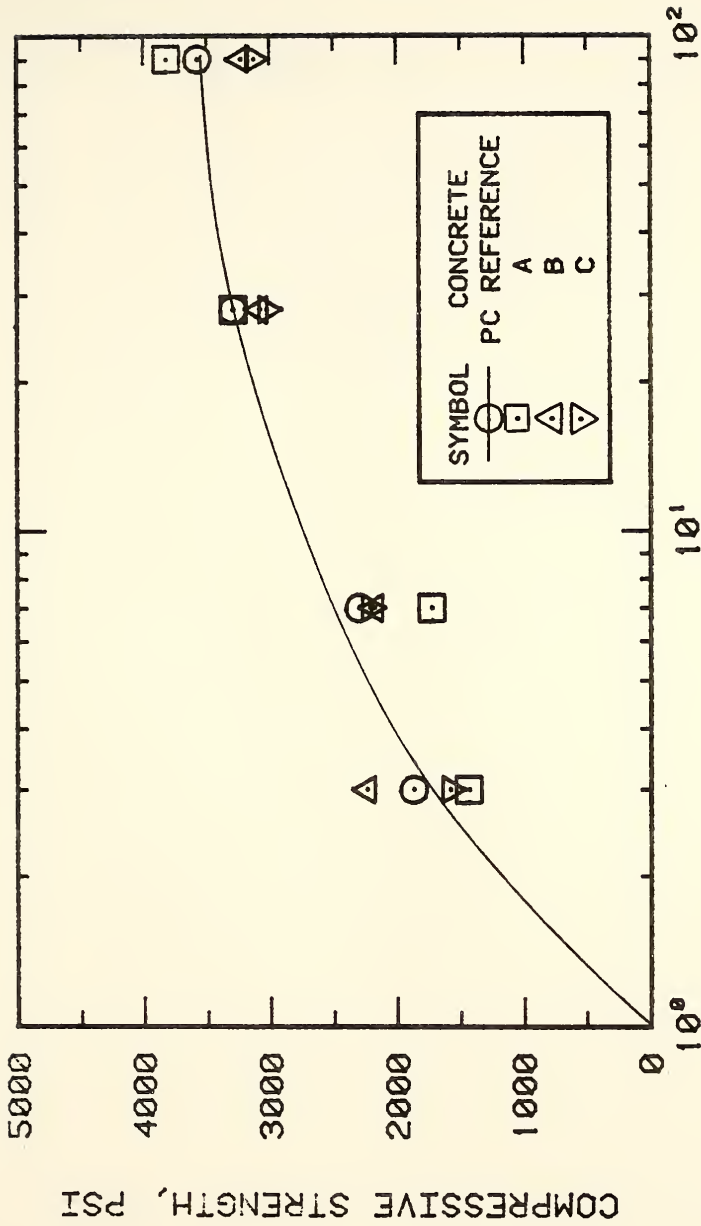
A tabulation of the development of compressive strength of concrete cylinders is given in Table 4-14. The values given represent the means of four tested cylinders and the corresponding standard deviations.

Table 4-14. Compressive strength of 3 X 6 in concrete cylinders prepared with different flyashes, Psi, and corresponding standard deviations shown in parentheses.

Age, days	Reference concrete	Systems				
		A	B	C	D	E
3	1870	1430	2230	1580	1220	1380
	(200)	(260)	(130)	(160)	(110)	(100)
7	2300	1720	2170	2210	1310	1610
	(270)	(420)	(100)	(250)	(100)	(180)
28	3290	3280	3070	3020	1930	2430
	(540)	(180)	(100)	(260)	(110)	(80)
90	3570	3810	3220	3120	2720	3130
	(360)	(640)	(310)	(290)	(410)	(670)

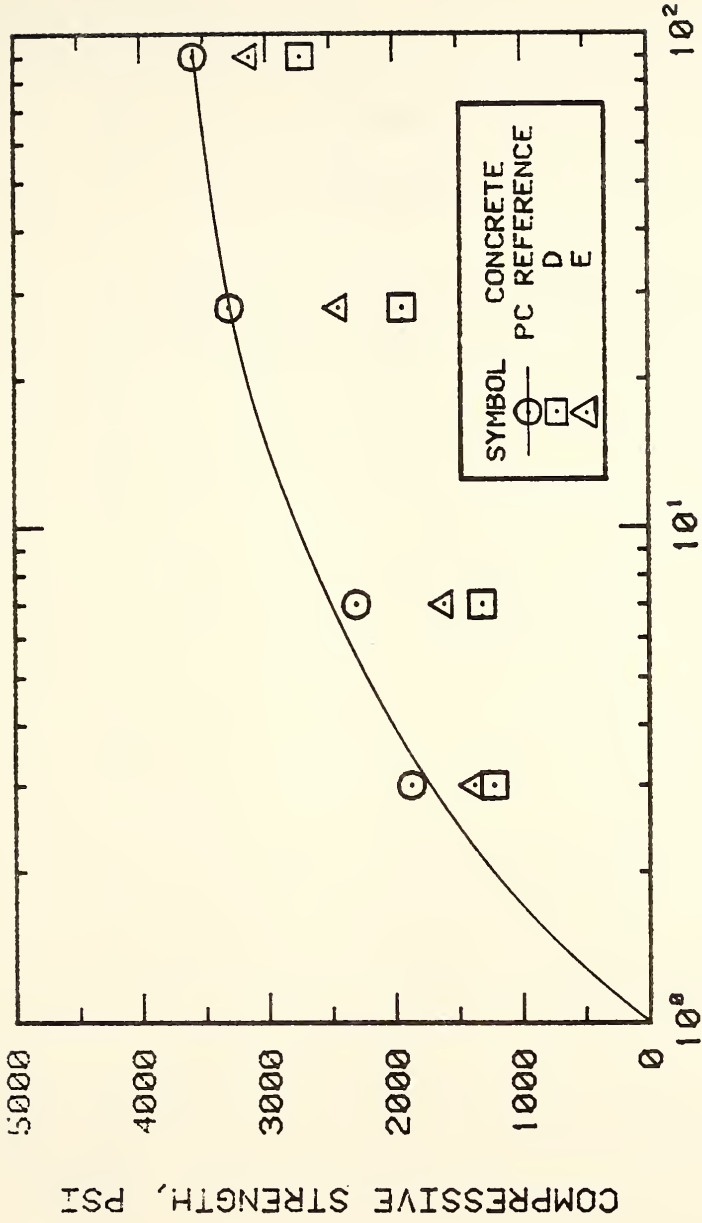
Figures 4-29 and 4-30 are plots of these data on a logarithmic time scale. There is a clear difference between the effects of the high-lime and the low-lime flyashes on the compressive strength of concrete cylinders. The concrete cylinders prepared with the low-lime flyashes, flyashes D and E, showed compressive strengths amounting to 60 and 70 percent, respectively, of the compressive strength of the portland cement reference concrete cylinders up to 28 days. The concrete cylinders tested at 90 days showed a compressive strength equivalent to 76 percent (system D concrete cylinders) and 88 percent (system E concrete cylinders) of the compressive strength of the reference concrete cylinders at the same age.

In contrast, the concrete cylinders prepared with the high-lime flyashes showed comparatively higher compressive strengths. Even though system A concrete cylinders have a slow start achieving strength, they show, at later ages, the highest compressive strengths of all the cylinders tested, including the reference concrete cylinders. This results are similar to those obtained for the compressive strength of system A mortar cubes. System B and C concrete cylinders showed compressive strengths slightly lower than the strengths of the reference concrete cylinders at all ages tested.



TIME, DAYS

Fig. 4-29. Compressive strengths of concrete cylinders bearing flyashes A, B, and C.



TIME, DAYS

Fig. 4-30. Compressive strengths of concrete cylinders bearing flyashes D and E.

CHAPTER 5

CONCLUSIONS

1. This study of five different flyashes indicates that not only are ASTM class C and class F flyashes different in composition, but that class C flyashes are more complex in nature and in reactivity with portland cement. The class C flyashes contain crystalline cementitious compounds that will react directly with water in the hydration process; the class F flyashes contain only inert crystalline compounds.
2. The sulfur, alkalis, and calcium found in the ASTM class C flyashes used in this study, and absent in the class F flyashes affect the reactions between class C flyashes and portland cement. These elements are found primarily in the form of water-soluble crystalline compounds.
3. The chemical composition of flyash particles varies as a function of particle size. This is true for both the class C flyashes and the class F flyash analyzed. The presence of large concentrations of calcium in the finest particles of the class C flyashes dramatically increases the potential reactivity of these materials.
4. The ASTM class F flyashes used in this study contribute to strength development only as a result of glass reaction, since the crystalline components are essentially all inert substances.
5. The glass in the class C flyashes shows a different type of x-ray scattering curve than the glass in the class F flyashes and may be expected to be more reactive.

6. Differences in the dormant period for pastes exist among different class C flyashes, and may be related to specific chemical differences, specifically the content of crystalline CaO and the content of alkalies present.

7. Early compressive strength development of concretes also differ among concretes with different class C flyashes, and these probably reflect the same compositional differences. Differences in the heat evolution patterns are also probably related to these compositional differences.

8. Differences in the alkali and sulfate contents of the pore solutions of flyash bearing pastes made with different class C flyashes also reflect these compositional differences. A class C flyash of low alkali and sulfate content generated pore solutions which did not vary very much from those of the reference cement pastes, but others with high concentrations of these components produced pore solutions rich in alkalies and sulfates. Subsequently these develop very high pH levels.

9. Flyash with low alkali contents are good choices for mixes where the alkali-aggregate reaction is a threat. Conversely flyashes with high alkali contents may be deleterious, especially if the alkalies are readily soluble. Soluble alkali contents of the order of 0.7 percent equivalent Na_2O or greater are likely to produce deleterious expansion with reactive aggregates.

BIBLIOGRAPHY

BIBLIOGRAPHY

1. McMillan, F. R. and Powers, T. C., "A method of evaluating admixtures", Proceedings American Concrete Institute, 30, p. 325, (1934).
2. Davis, R. E., Carlson, R. W., Kelly, J. W., and Davis, H. E., "Properties of cements and concretes containing flyash", Proceedings American Concrete Institute, 33, p. 577, (1937).
3. Lovewell, C. E. and Washa, G. W., "Proportioning concrete mixtures using flyash", Proceedings American Concrete Institute, 54, p. 1093, (1957-58).
4. Mielenz, R. C., "Specifications and methods of using flyash in portland cement concrete", Proceedings Third International Ash Utilization Symposium, Pittsburgh, Pa., p. 61, (1973).
5. American Society for Testing and Materials, Designation D 388-77 "Standard classification of coals by rank", Annual Book of ASTM standards, Part 26, p. 212, (1981).
6. Mazza, M. H. and Wilson, J. S., "X-ray diffraction examination of coal combustion products related to boiler tube fouling and slagging", Advances in X-ray Analysis, 20, p. 85, (1976).
7. Gibbon, D. L., "Microcharacterization of flyash and analogs: the role of SEM and TEM", Scanning Electron Microscopy, SEM Inc., p. 501, (1979).
8. Berry, E. E., "Flyash for use in concrete. Part I - a critical review of the chemical, physical, and pozzolanic properties of flyash", Mineral Sciences Laboratories CANMET Report 76-25, (August 1976).
9. American Society for Testing and Materials, Designation C 618-80 "Standard specification for flyash and raw or calcined natural pozzolan for use as a mineral admixture in portland cement concrete", Annual Book of ASTM standards, Part 14, p. 362, (1979).

10. Watt, J. D. and Thorne, D. J., "Composition and pozzolanic properties of pulverized fuel ashes. I. Composition of flyashes from some British power stations and properties of their component particles", *Journal of Applied Chemistry*, 15, p. 585, (1965).
11. Mateos, M. and Davidson, D. J., "Steam curing and x-ray studies of flyash", *Proceedings American Society for Testing and Materials*, 62, p. 1008, (1962).
12. Minnick, L. J., "Reactions of hydrated lime with pulverized coal flyash", *Proceedings Symposium on Flyash Utilization, Pittsburgh, Pa.*, p. 287, (1967).
13. Mitchell, R. S. and Gluskoter, H. J., "Mineralogy of ash of some American coals: variations with temperature and source", *Fuel, London*, 55, p. 90, (1976).
14. Minnick, L. J., "The new flyash", *Proceedings Second Ash Utilization Symposium, Pittsburgh, Pa.*, p. 269, (1970).
15. Natusch, D. F. S., "Characterization of atmospheric pollutants from power plants", *Second Federal Conference on the Great Lakes. Michigan*, p. 114, (1976).
16. Raask, E., "Cenospheres in pulverized-fuel ash", *Journal of the Institute of Fuel*, 41, Sept. No. 332, p. 339, (1968).
17. Fisher, G. L., Chang, D. P. Y., and Brummer, M., "Flyash collected from electrostatic precipitators: microcrystalline structures and the mystery of the spheres", *Science*, 192, p. 553, (1976).
18. Raask, E. and Street, P. J., "Appearance and pozzolanic activity of pulverized fuel ash", *Conference on Ash Technology and Marketing, Paper 4.9*, (1978).
19. Brink, R. H. and Halstead, W. J., "Studies relating to the testing of flyash for use in concrete", *Proceedings American Society for Testing and Materials*, 56, p. 1161, (1956).
20. Smith, M. A. and Halliwell, F., "The application of the BS 4550 test for pozzolanic cements to test cement containing pulverized fuel ashes", *Magazine of Concrete Research*, 31, No. 108, p. 159, (1979).

21. Thorne, D. J. and Watt, J. D., "Composition and pozzolanic properties of pulverized fuel ashes. II. Pozzolanic properties of flyashes, as determined by crushing tests on lime mortars", Journal of Applied Chemistry, 15, p. 595, (1965).
22. Rehsi, S. S., "Studies of Indian flyashes and their use in structural concrete", Proceedings Third International Ash Utilization Symposium, Pittsburgh, Pa., p. 231, (1973).
23. Raask, E. and Bhaskar, M. C., "Pozzolanic activity of pulverized fuel ash", Cement and Concrete Research, 5, p. 363, (1975).
24. Kovacs, R., "Effects of the hydration products on the properties of flyash cements", Cement and Concrete Research, 5, p. 73, (1975).
25. Matthews, J. D. and Gutt, W. H., "Studies of flyash as a cementitious material", Conference on Ash Technology and Marketing, Paper 4.10, (1978).
26. Watt, J. D. and Thorne, D. J., "The composition and pozzolanic properties of pulverized fuel ashes. III. Pozzolanic properties of flyashes as determined by chemical methods", Journal of Applied Chemistry, 16, p. 33, (1966).
27. Kokubu, M., "Flyash and flyash cement", Proceedings Fifth International Symposium on Chemistry of Cement, Tokyo, Japan, Part 4, p. 75, (1968).
28. Cabrera, J. G. and Plowman, C., "The influence of pulverized fuel ash on the early and long term strength of concrete", Proceedings Seventh International Congress on the Chemistry of Cement, Paris, France, Part 4, p. 84, (1980).
29. Kocuvan, I., "A proposal for classification of flyashes", Proceedings Fifth International Ash Utilization Symposium, Atlanta, Georgia, Part 1, p. 215, (1979).
30. Mielenz, R. C., "Specifications on flyash for use in concrete: where we are - where should we go?" Proceedings Fifth International Ash Utilization Symposium, Part 2, p. 482, (1979).
31. Owens, P. L., "Flyash and its usage in concrete", Concrete, 13, No. 7, p. 21, (1979).

32. Berry, E. E. and Malhotra, V. M., "Flyash for use in concrete. Part II - a critical review of the effects of flyash on the properties of concrete", Mineral Sciences Laboratories CANMET Report 78-16, (1978).
33. Gosh, R. S., "Proportioning of concrete mixes incorporating flyash", Canadian Journal of Civil Engineering, 3, p. 68, (1976).
34. Mindess, S. and Young, J. F., "Concrete," Prentice Hall, Inc., First edition, New Jersey, (1981).
35. Popovics, S., "Strength relationships for flyash concrete", Journal American Concrete Institute, 79, No. 1, p. 43, (1982).
36. Kokubu, M., "Selected papers of Masatane Kokubu", Transactions Japan Society of Civil Engineers, No. 71, p. 125, (1975).
37. Davis, R. E., "Pozzolanic materials - with special reference to their use in concrete pipe", American Concrete Pipe Association, Technical Memo, (1954).
38. Dunstan Jr., E. R., "Performance of lignite and sub-bituminous flyash in concrete - a progress report", Bureau of Reclamation Engineering and Research Center, Denver, Colorado, (Jan. 1976).
39. Manz, O. E., "Ash from lignite", Proceedings Second Ash Utilization Symposium, Pittsburgh, Pa., p. 282, (1970).
40. Minnick, L. J., "Reactions of calcium and magnesium compounds with pulverized coal flyash", Pres. Ann. Meeting AIME, N. Y., (Feb. 1968).
41. Stanton, T. E., "Expansion of concrete through reaction between cement and aggregate", American Society of Civil Engineers, 66, p. 1781, (1940).
42. Pepper, L. and Mather, B., "Effectiveness of mineral admixtures in preventing excessive expansion of concrete due to alkali-aggregate reaction", Proceedings American Society for Testing and Materials, 59, p. 1178, (1959).
43. Diamond, S. "A review of alkali-silica reaction and expansion mechanism: Part I, alkalies in cement and in concrete pore solutions", Cement and Concrete Research, 5, No. 4, p. 329, (1975).

44. Chatterji, S., "The role of Ca(OH)_2 in the breakdown of portland cement concrete due to alkali-silica reaction", Cement and Concrete Research, 9, NO. 2, p. 185, (1979).
45. Diamond, S., "Effects of two Danish flyashes on alkali contents of pore solutions of cement-flyash pastes", Cement and Concrete Research, 11, No. 3, p. 383, (1981).
46. Gutt, W., Nixon, P. J., and Gaza, M. E., "Observations of the mechanism by which flyash reduces expansion due to alkali-aggregate reaction", Seventh International Congress on the Chemistry of Cement, (1980).
47. Barneyback Jr., R. S. and Diamond, S., "Expression and analysis of pore fluids from hardened cement pastes and mortars", Cement and Concrete Research, 11, p. 279, (1981).

APPENDICES

Appendix A. Chemical Composition of Flyash C

Table A-1. Wet chemical analysis of flyash C.*

<u>Oxide</u>	<u>Percent</u>
CaO	22.25
SiO ₂	27.92
Al ₂ O ₃	11.62
Fe ₂ O ₃	11.58
MgO	6.88
Na ₂ O	6.30
K ₂ O	0.68
SO ₃	6.09
TiO ₂	0.40
P ₂ O ₅	0.40
Cl	0.19
Mn ₂ O ₃	0.19
LOI	1.59
	<hr/>
	95.90

* Reported by Dr. Jan Skalny, Martin Marietta Laboratories.

Appendix B. X-Ray Diffraction Patterns of the Flyashes Used

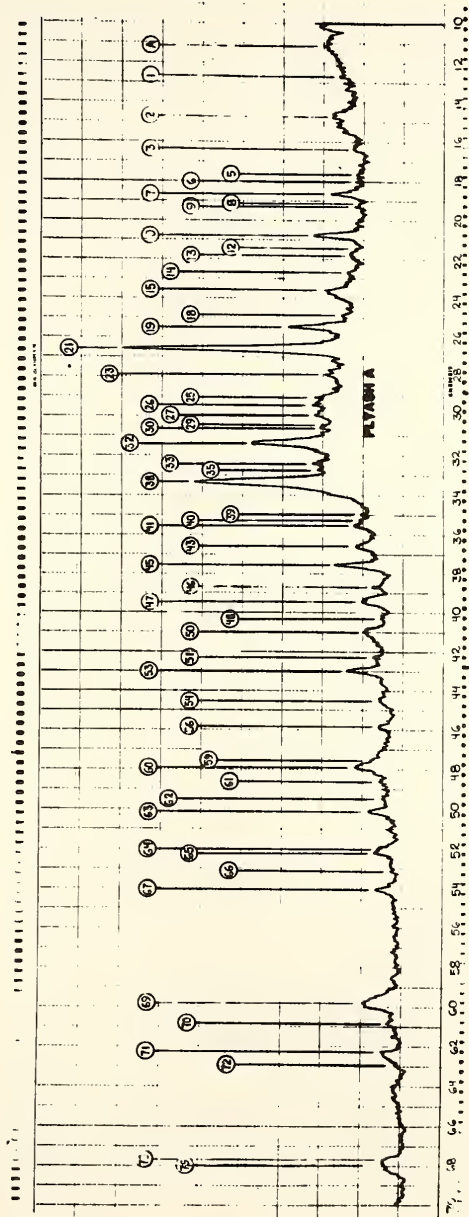


Fig. B-1. X-ray diffraction pattern for flyash A.

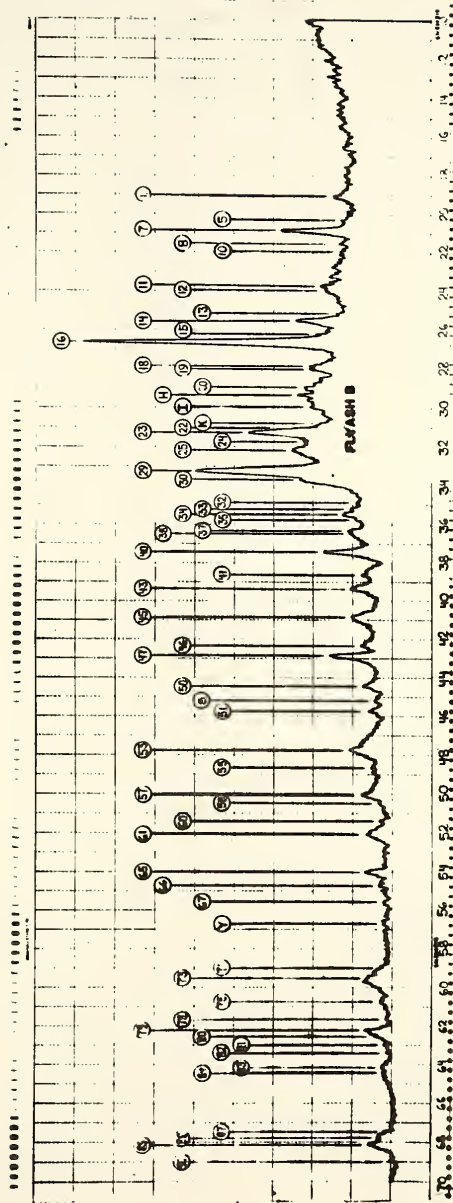


Fig. B-2. X-ray diffraction pattern for flyash B.

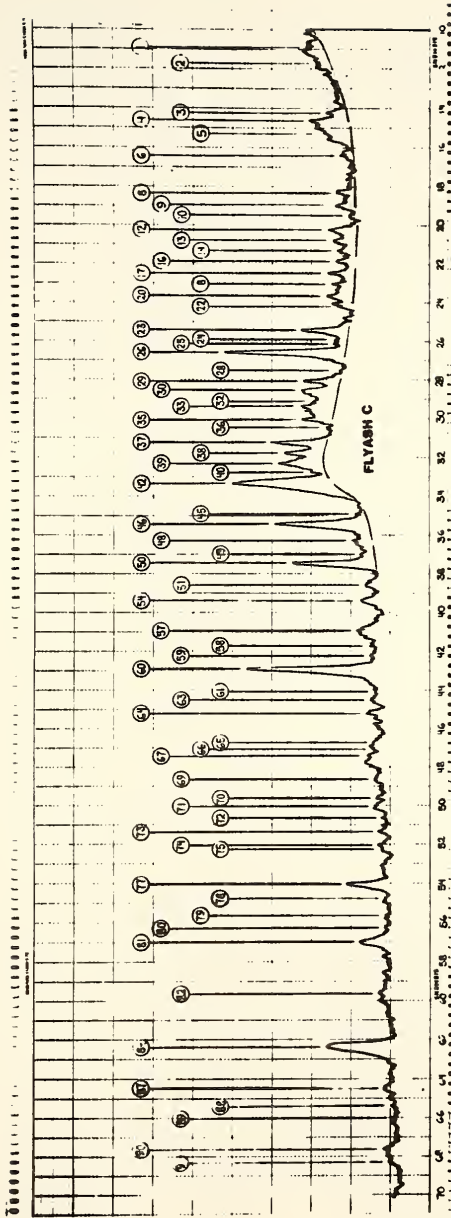


Fig. B-3. X-ray diffraction pattern for flyash C.

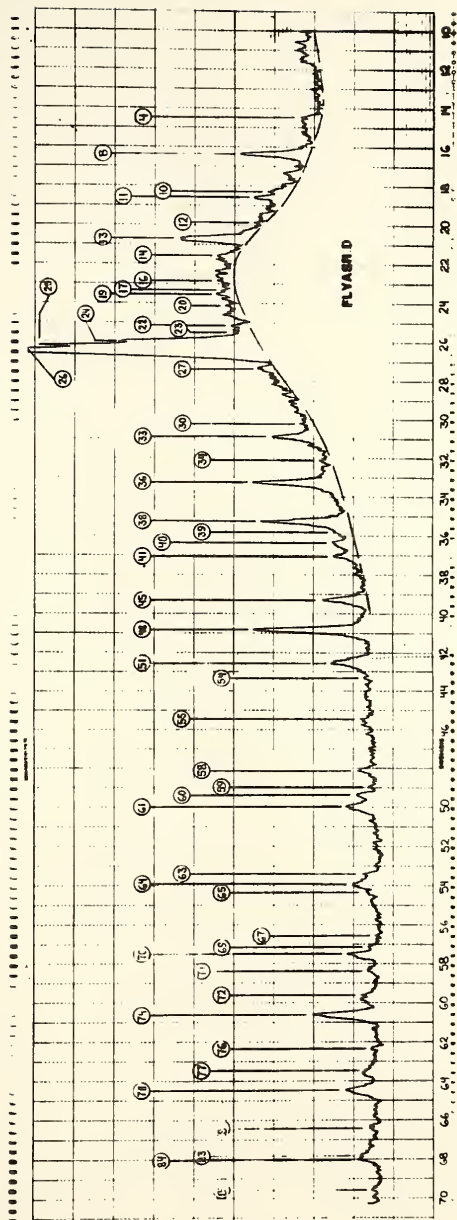


Fig. B-4. X-ray diffraction pattern for flyash D.

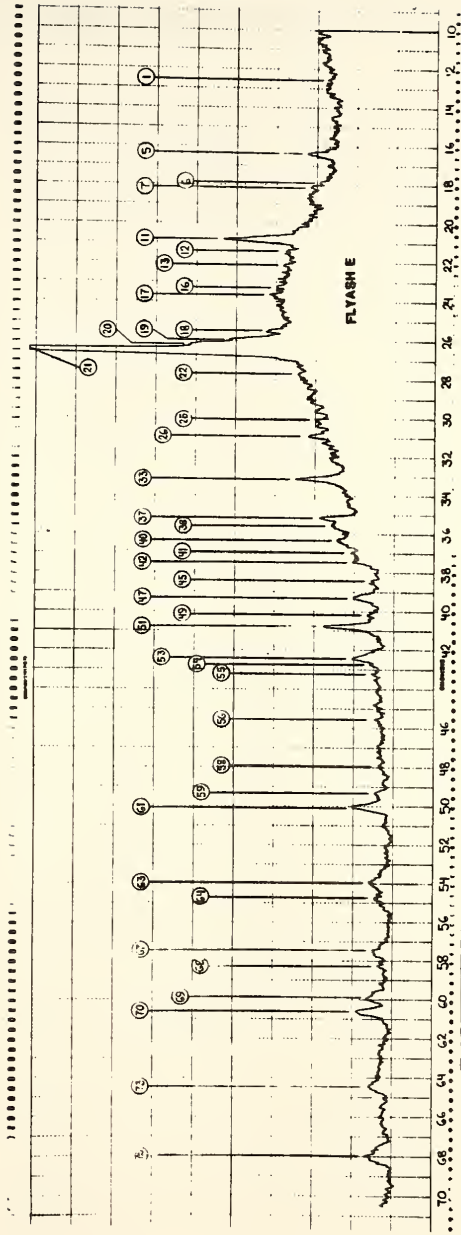


Fig. B-5. X-ray diffraction pattern for flyash E.

Appendix C. Chemical Analyses of Paste Pore Solutions

Table C-1. Measured normality of ionic species in paste pore solutions as a function of time (not adjusted for change in water content).

Reference Portland Cement Paste

<u>Age, hours</u>	<u>Ca²⁺</u>	<u>K⁺</u>	<u>Na⁺</u>	<u>SO₄²⁻</u>	<u>OH⁻</u>	<u>Charge balance</u>
1	0.0480	0.3004	0.0329	0.1770	0.1657	+ .0386
2	0.0460	0.3005	0.0336	0.1736	0.1639	+ .0426
4	0.0446	0.3031	0.0347	0.1906	0.1597	+ .0321
6	0.0424	0.3069	0.0357	0.2084	0.1528	+ .0238
10	0.0404	0.3094	0.0365	0.2084	0.1466	+ .0313
14	0.0123	0.3222	0.0384	0.0864	0.2592	+ .0273
18	0.0078	0.3272	0.0384	0.0438	0.3187	+ .0109
24	0.0066	0.3350	0.0389	0.0260	0.3522	+ .0023
72	0.0068	0.3453	0.0465	0	0.4091	- .0105
168	0.0060	0.3579	0.0483	0	0.4338	- .0216
672	0.0027	0.3862	0.0635	0	0.4515	+ .0009
2160	0	0.3941	0.0638	0	0.4290	+ .0289
4320	0	0.3840	0.0563	0	0.4099	+ .0304

Table C-2. Measured normality of ionic species in paste pore solutions as a function of time (not adjusted for change in water content).

Paste with Flyash A						
<u>Age, hours</u>	<u>Ca²⁺</u>	<u>K⁺</u>	<u>Na⁺</u>	<u>SO₄²⁻</u>	<u>OH⁻</u>	<u>Charge balance</u>
1	0.0434	0.2097	0.0315	0.1406	0.1252	+ .0188
2	0.0476	0.2124	0.0328	0.1322	0.1386	+ .0220
4	0.0440	0.2097	0.0338	0.1552	0.1436	- .0113
6	0.0430	0.2097	0.0340	0.1731	0.1428	- .0292
10	0.0446	0.2174	0.0355	0.1416	0.1371	+ .0188
14	0.0108	0.2366	0.0405	0.0198	0.2604	+ .0077
18	0.0086	0.2481	0.0450	0	0.2921	+ .0096
24	0.0080	0.2481	0.0465	0	0.2949	+ .0077
72	0.0056	0.2864	0.0821	0	0.3793	- .0052
168	0.0058	0.2992	0.1012	0	0.4298	- .0236
672	0.0026	0.3102	0.1412	0	0.4579	- .0039
2160	0	0.3001	0.1693	0	0.4412	+ .0282
4320	0	0.2944	0.1537	0	0.4302	+ .0179

Table C-3. Measured normality of ionic species in paste pore solutions as a function of time (not adjusted for change in water content).

Age, hours	Paste with Flyash B					Charge balance
	Ca ²⁺	K ⁺	Na ⁺	SO ₄ ²⁻	OH ⁻	
1	0.0425	0.1985	0.2936	0.3416	0.1663	+0.0267
3	0.0426	0.1985	0.2936	0.3350	0.1788	+0.0209
6	0.0286	0.2133	0.3045	0.3184	0.2010	+0.0227
10	0.0060	0.2188	0.3132	0.0377	0.4714	+0.0289
14	0.0040	0.2291	0.3197	0	0.5447	+0.0081
18	0.0044	0.2327	0.3241	0	0.5598	+0.0014
24	0.0038	0.2354	0.3262	0	0.5567	+0.0087
72	0.0046	0.2634	0.3445	0	0.6242	-0.0117
168	0.0038	0.2762	0.3672	0	0.6737	-0.0265
672	0.0024	0.2813	0.4350	0	0.7009	+0.0178
2160	0	0.2744	0.4385	0	0.6226	+0.0903
4320	0	0.2719	0.4141	0	0.6056	+0.0804

Table C-4. Measured normality of ionic species in paste pore solutions as a function of time (not adjusted for change in water content).

Paste with Flyash C						
<u>Age, hours</u>	<u>Ca²⁺</u>	<u>K⁺</u>	<u>Na⁺</u>	<u>SO₄²⁻</u>	<u>OH⁻</u>	<u>Charge balance</u>
1	0.0460	0.2157	0.4132	0.4292	0.1885	+0.0572
3	0.0450	0.2161	0.4132	0.4242	0.1955	+0.0546
6	0.0410	0.2189	0.4132	0.4416	0.1780	+0.0535
10	0.0153	0.2340	0.4350	0.3438	0.2888	+0.0517
14	0.0070	0.2327	0.4219	0.1501	0.4343	+0.0772
18	0.0038	0.2418	0.4219	0.0458	0.6160	+0.0057
24	0.0030	0.2545	0.4393	0.0152	0.6785	+0.0031
72	0.0036	0.2762	0.4838	0	0.7626	+0.0010
168	0.0034	0.2813	0.5350	0	0.8307	-0.0110
672	0.0022	0.3197	0.6725	0	0.9772	+0.0172
2160	0	0.3404	0.8165	0	1.0458	+0.1111
4320	0	0.3419	0.7057	0	0.9944	+0.0532

Table C-5. Measured normality of ionic species in paste pore solutions as a function of time (not adjusted for change in water content).

Paste with Flyash D						
Age, hours	Ca ²⁺	K ⁺	Na ⁺	SO ₄ ²⁻	OH ⁻	Charge balance
1	0.0493	0.1935	0.0229	0.1155	0.1350	+0.0152
3	0.0476	0.1950	0.0228	0.1178	0.1310	+0.0166
6	0.0444	0.1932	0.0249	0.1312	0.1260	+0.0053
10	0.0202	0.1988	0.0255	0.0620	0.1580	+0.0245
14	0.0118	0.2092	0.0263	0.0446	0.2160	-0.0133
18	0.0086	0.2145	0.0267	0.0206	0.2450	-0.0158
24	0.0078	0.2238	0.0278	0.0235	0.2640	-0.0281
72	0.0052	0.2532	0.0395	0	0.2940	+0.0039
168	0.0056	0.2532	0.0379	0	0.3081	-0.0114
672	0.0040	0.2455	0.0413	0	0.2824	+0.0084
2160	0	0.2225	0.0529	0	0.2692	+0.0062
4320	0	0.2188	0.0572	0	0.2400	+0.0360

Table C-6. Measured normality of ionic species in paste pore solutions as a function of time (not adjusted for change in water content).

Paste with Flyash E						
<u>Age, hours</u>	<u>Ca²⁺</u>	<u>K⁺</u>	<u>Na⁺</u>	<u>SO₄²⁻</u>	<u>OH⁻</u>	<u>Charge balance</u>
1	0.0546	0.1967	0.0242	0.1142	0.1455	+ .0158
3	0.0492	0.1976	0.0244	0.1155	0.1375	+ .0182
6	0.0452	0.2001	0.0252	0.1292	0.1256	+ .0157
10	0.0290	0.2061	0.0259	0.0976	0.1510	+ .0124
14	0.0163	0.2082	0.0270	0.0608	0.1915	+ .0008
18	0.0108	0.2120	0.0272	- - -	0.2215	+ .0285
24	0.0074	0.2187	0.0281	0.0165	0.2555	- .0198
72	0.0060	0.2532	0.0363	0	0.2990	- .0035
168	0.0065	0.2633	0.0397	0	0.3217	- .0122
672	0.0052	0.2761	0.0472	0	0.3206	+ .0079
2160	0	0.2771	0.0515	0	0.3240	+ .0046
4320	0	0.2751	0.0427	0	0.2890	+ .0288

Appendix D. Length Change Results for Mortar Bars

Table D-1. Length changes in reference portland cement mortar bars, percent strain.

Age, days	Length change in percent strain			
	1	2	3	4
1	0	0	0	0
2	-0.0041	-0.0033	-0.0025	-0.0005
3	-0.0039	-0.0030	-0.0022	-0.0002
4	-0.0065	-0.0062	-0.0057	-0.0038
5	-0.0065	-0.0057	-0.0058	-0.0045
6	-0.0086	-0.0076	-0.0067	-0.0058
7	-0.0103	-0.0102	-0.0096	-0.0083
11	-0.0103	-0.0095	-0.0099	-0.0079
18	-0.0125	-0.0096	-0.0089	-0.0072
25	-0.0105	-0.0099	-0.0101	-0.0103
32	-0.0084	-0.0081	-0.0089	-0.0113
60	-0.0101	-0.0091	-0.0086	-0.0078
109	-0.0122	-0.0106	-0.0100	-0.0086
194	-0.0088	-0.0069	-0.0058	-0.0045
250	-0.0109	-0.0084	-0.0077	-0.0062
319	-0.0147	-0.0129	-0.0144	-0.0116

Table D-2. Length changes in system A cement-flyash mortar bars,
percent strain.

Age, days	1				2				3				4			
	0	0.0037	0	0.0011	0	0.0011	0	0.0023	0	0.0013	0	0.0023	0	0.0015		
2	0.0010	0.0010	-0.0001	-0.0001	-0.0001	-0.0001	0.0003	0.0003	0.0003	0.0003	0.0003	0.0003	0.0003	0.0018		
3	0.0016	0.0016	-0.0012	-0.0012	-0.0012	-0.0012	-0.0026	-0.0026	-0.0026	-0.0026	-0.0026	-0.0026	-0.0026	0.0069		
4	0.0015	0.0015	-0.0014	-0.0014	-0.0014	-0.0014	-0.0045	-0.0045	-0.0045	-0.0045	-0.0045	-0.0045	-0.0045	0.0089		
5	-0.0064	-0.0064	-0.0090	-0.0090	-0.0090	-0.0090	-0.0125	-0.0125	-0.0125	-0.0125	-0.0125	-0.0125	-0.0125	0.0182		
7	-0.0086	-0.0086	-0.0096	-0.0096	-0.0096	-0.0096	-0.0134	-0.0134	-0.0134	-0.0134	-0.0134	-0.0134	-0.0134	0.0205		
10	-0.0128	-0.0128	-0.0125	-0.0125	-0.0125	-0.0125	-0.0159	-0.0159	-0.0159	-0.0159	-0.0159	-0.0159	-0.0159	0.0224		
17	-0.0180	-0.0180	-0.0137	-0.0137	-0.0137	-0.0137	-0.0148	-0.0148	-0.0148	-0.0148	-0.0148	-0.0148	-0.0148	0.0187		
24	-0.0226	-0.0226	-0.0188	-0.0188	-0.0188	-0.0188	-0.0152	-0.0152	-0.0152	-0.0152	-0.0152	-0.0152	-0.0152	0.0188		
32	-0.0135	-0.0135	-0.0178	-0.0178	-0.0178	-0.0178	-0.0218	-0.0218	-0.0218	-0.0218	-0.0218	-0.0218	-0.0218	0.0234		
60	-0.0163	-0.0163	-0.0219	-0.0219	-0.0219	-0.0219	-0.0255	-0.0255	-0.0255	-0.0255	-0.0255	-0.0255	-0.0255	0.0295		
109	-0.0209	-0.0209	-0.0215	-0.0215	-0.0215	-0.0215	-0.0219	-0.0219	-0.0219	-0.0219	-0.0219	-0.0219	-0.0219	0.0231		
194	-0.0212	-0.0212	-0.0217	-0.0217	-0.0217	-0.0217	-0.0224	-0.0224	-0.0224	-0.0224	-0.0224	-0.0224	-0.0224	0.0232		
250	-0.0221	-0.0221	-0.0225	-0.0225	-0.0225	-0.0225	-0.0239	-0.0239	-0.0239	-0.0239	-0.0239	-0.0239	-0.0239	0.0241		
319																

Table D-3. Length changes in system B cement-flyash mortar bars, percent strain.

Age, days	1	2	3	4
1	0	0	0	0
2	0.0011	0.0008	0.0020	0.0023
3	0.0001	-0.0012	0.0005	0.0007
4	0.0021	0.0001	0.0016	0.0016
5	0.0011	-0.0011	0.0004	-0.0002
7	-0.0039	-0.0060	-0.0040	-0.0037
10	-0.0033	-0.0050	-0.0025	-0.0024
17	-0.0025	-0.0042	-0.0025	-0.0027
24	-0.0022	-0.0022	-0.0010	-0.0012
31	-0.0039	-0.0053	-0.0035	-0.0035
60	0.0017	0.0003	0.0013	0.0013
109	0.0013	0.0002	0.0016	0.0001
194	0.0051	0.0039	0.0049	0.0048
250	0.0077	0.0071	0.0081	0.0076
319	0.0086	0.0080	0.0089	0.0081

Table D-4. Length changes in system C cement-flyash mortar bars, percent strain.

Age, days	1	2	3	4
1	0	0	0	0
2	0.0015	0.0020	0.0025	0.0025
3	0.0030	0.0027	0.0029	0.0014
4	0.0054	0.0056	0.0054	0.0029
5	0.0043	0.0045	0.0045	-0.0024
7	-0.0036	-0.0002	0	-0.0077
10	-0.0012	0.0022	0	-0.0090
17	-0.0008	0.0026	-0.0012	-0.0123
24	-0.0071	0.0005	0.0019	-0.0025
31	-0.0052	0.0015	0.0019	-0.0019
60	0.0070	0.0093	0.0091	0.0105
109	0.0190	0.0339	0.0279	0.0213
194	0.0371	0.0528	0.0397	0.0297
250	0.0429	0.0580	0.0471	0.0420
319	0.0445	0.0604	0.0485	0.0453

Table D-5. Length changes in system D cement-flyash mortar bars, percent strain.

Age, days	Length changes in system D cement-flyash mortar bars, percent strain.			
	1	2	3	4
1	0	0	0	0
2	-0.0026	-0.0026	-0.0025	-0.0014
3	-0.0024	-0.0030	-0.0022	-0.0012
4	-0.0034	-0.0040	-0.0040	-0.0031
5	-0.0051	-0.0042	-0.0028	-0.0019
6	-0.0055	-0.0060	-0.0064	-0.0075
7	-0.0081	-0.0101	-0.0122	-0.0157
11	-0.0086	-0.0095	-0.0125	-0.0169
18	-0.0092	-0.0115	-0.0158	-0.0205
25	-0.0094	-0.0135	-0.0185	-0.0243
32	-0.0125	-0.0147	-0.0186	-0.0260
60	-0.0085	-0.0101	-0.0138	-0.0171
109	-0.0116	-0.0124	-0.0152	-0.0182
194	-0.0098	-0.0098	-0.0122	-0.0142
250	-0.0091	-0.0010	-0.0126	-0.0136
319	-0.0167	-0.0183	-0.0199	-0.0210

Table D-6. Length changes in system E cement-flyash mortar bars, percent strain.

Age, days	1	2	3	4
1	0	0	0	0
2	-0.0017	-0.0015	-0.0028	-0.0038
3	-0.0007	-0.0006	-0.0015	-0.0048
4	-0.0020	-0.0011	-0.0028	-0.0053
5	-0.0002	-0.0005	-0.0021	-0.0067
6	-0.0023	-0.0035	-0.0053	-0.0104
7	-0.0072	-0.0097	-0.0138	-0.0195
11	-0.0102	-0.0094	-0.0117	-0.0156
18	-0.0179	-0.0159	-0.0148	-0.0183
25	-0.0180	-0.0155	-0.0165	-0.0213
32	-0.0165	-0.0153	-0.0188	-0.0238
60	-0.0205	-0.0201	-0.0221	-0.0259
109	-0.0209	-0.0212	-0.0224	-0.0260
194	-0.0692	-0.0684	-0.0724	-0.0685
250	-0.0306	-0.0311	-0.0326	-0.0314
319	-0.0323	-0.0335	-0.0352	-0.0326

COVER DESIGN BY ALDO GIORGINI